Hot Working and Recrystallization of As-Cast 316L

MARTIN C. MATAYA, ERIC R. NILSSON, ELLIOT L. BROWN, and GEORGE KRAUSS

Stress-strain behavior and microstructure evolution during hot working of as-cast austenitic stainless steel alloy 316L were investigated by uniaxial compression of cylindrical specimens at a strain rate of 1 s^{-1} over the temperature range 1000 °C to 1150 °C and up to a strain of one. The measured flow curves showed monotonic hardening, indicating that dynamic recrystallization was not important in microstructural evolution. Static recrystallization was observed to nucleate preferentially at the delta ferrite-austenite interphase boundaries. The recrystallization kinetics of the as-cast material was compared to a relatively fine-grained wrought 316L material and found to be somewhat slower. However, the difference between the two material conditions was not nearly as great as previously reported for as-cast and wrought 304L alloy. The difference in behaviors between 316L and 304L is attributed to the relatively large amount and vermicular morphology of the delta ferrite phase in the 316L, resulting in a relatively fine effective grain size, compared to the existing coarse columnar structure, and concomitant enhancement of recrystallization. Compared to wrought 316L, the recrystallization rate of the as-cast material was relatively sluggish, despite a relatively fine effective grain size. The difference is associated with the 100 orientations of the columnar grains with respect to the compression axis, producing a soft orientation and a reduced rate of accumulation of dislocation density in the substructure. Also, compared to wrought 316L, the recrystallization rate of the as-cast material tends to decrease with time, the drop occurring concurrently with spheroidization and dissolution of the ferrite. It is suggested that (1) movement of the delta ferrite-austenite interphase boundary during spheroidization may poison incipient recrystallization and (2) dissolution of delta ferrite can locally enrich the austenite matrix in Mo and Cr, raising the local stacking fault energy and lowering grain boundary mobility to favor recovery over recrystallization in the vicinity of the ferrite-austenite boundary. A kinetic model for recrystallization was developed and used to simulate evolution of the first cycle of recrystallization during various thermal-mechanical treatment schedules typically employed during the primary breakdown of as-cast material.

I. INTRODUCTION

RECRYSTALLIZATION of coarse as-cast ingot structure in stainless steels is a primary objective during the initial stages of ingot breakdown. Incipient recrystallization at grain boundaries, where solute and second phases collect during solidification and cooling of ingots, enhances hot workability by reducing the propensity for the phenomenon of slivering and for crack formation at columnar grain boundaries. Hot working of ingot material occurs either by radial forging or open die pressing to produce billet and bar or by rolling of ingot or continuously cast slab to produce plate and sheet. Recrystallization is encouraged by the progressive accumulation of internal strain during the multiple pass sequences and occurs during the interpass periods or during subsequent reheating of the workpiece.

The rate of strain accumulation in the microstructure depends upon the local strain rate and temperature, microstructural characteristics, and stacking fault energy (SFE). As SFE increases, deformation can be more readily accommodated by the formation of low energy dislocation substructures that form by dislocation cross-slip and climb, mechanisms which are favored if stacking faults are not prevalent. For example, recovery processes dominate microstructural evolution in materials with high SFE, *e.g.*, Al, Zr, Ti, α-Fe, and ferritic steels, giving stable dislocation substructures that resist recrystallization. In materials with relatively low SFE, *e.g.*, Cu, CuAl, CuZn, Ag, Ni-Fe, Co, Ni-base superalloys, tool steels, and austenitic stainless steels, cross-slip is limited and recrystallization favored during conventional hot working processes.[1,2] Static recrystallization, rather than dynamic recrystallization, is the dominant restoration mechanism in conventional thermal-mechanical treatment. Dynamic recrystallization has been observed in low SFE materials (*e.g.*, 304L) during the application of large, continuous strain at low strain rate and high temperature, conditions atypical of conventional processing.[3]

Studies of microstructural evolution during primary breakdown of as-cast ingot and continuously cast structures have been limited because of the difficulty and expense in conducting pilot studies on subscale ingots or in obtaining test specimens from large as-cast commercial ingots. In addition, inhomogeneous deformation of test specimens may result from the relatively large grains or preferred crystallographic texture associated with columnar grain structure typical in conventional ingots and continuous cast slabs.[4,5] Inhomogeneous deformation, in turn, causes localized gradients in the test specimen microstructure due to high gradients in strain (ε), strain rate ($\dot{\varepsilon}$), and temperature (T). Under these conditions, accurate measurements of the volume fraction

MARTIN C. MATAYA is Technical Staff Member, Los Alamos National Laboratory, and Research Professor, Advance Steel Processing and Products Research Center (ASPPRC), Colorado School of Mines, Golden, Co. 80403. Contact e-mail: mataya@lanl.gov ERIC R. NILSSON, formerly Graduate Student, ASPPRC, is Faculty Member, Baker College, Cadillac, MI 49601. ELLIOT L. BROWN is President, EB Scientific Enterprises, Golden, CO 80403. GEORGE KRAUSS is University Emeritus Professor with Colorado School of Mines, and Past Director, ASPPRC.

Manuscript submitted June 7, 2002.

recrystallized as well as the association of the measurements with deformation parameters is very difficult. Therefore, nearly all of the investigations of microstructural evolution in austenitic stainless steels during hot working have been conducted on wrought, fully recrystallized material with relatively fine grains.

Although data sets from fully recrystallized steels are useful in modeling microstructural evolution during the latter stages of ingot breakdown, after one or more cycles of recrystallization have taken place, their applicability with respect to the initial stages of breakdown is restricted. For example, Campbell *et al*.[6] compared the recrystallization kinetics of as-cast AISI 304 stainless steel to wrought and annealed (recrystallized) material from the same heat and showed that the ingot structure recrystallized at a much slower rate. For $\varepsilon = 0.15$ at 1037 °C at a $\dot{\varepsilon}$ of 6 s^{-1}, the time for 80 pct recrystallization was 2800 and 65 seconds, respectively. Recrystallization was found to nucleate preferentially at high-angle grain boundaries in both conditions and the difference in kinetics was related directly to the difference in grain size between the two conditions.

In another study, Kane[7] found that in as-cast AISI type 310 alloy, recrystallization nucleated at δ-ferrite islands as well as columnar grain boundaries and that the volume fraction recrystallized increased with volume fraction δ. Ryan and Mc Queen[8] described the effective grain size in as-cast stainless steel, when considering recrystallization, to be on the order of the secondary dendrite arm spacing, assuming a network of interdendritic δ. In this light, the as-cast material studied by Campbell *et al*.,[6] which exhibited very little δ due to the application of a homogenization heat treatment, probably would have recrystallized more quickly if δ was more prevalent in the starting microstructure, prior to hot working. Thus, recrystallization of ingot material during primary breakdown is sensitive to the starting as-cast microstructure and cannot be accurately modeled utilizing wrought material behavior. Further, recrystallization in as-cast stainless steels appears to depend on the amount and probably the morphology of δ in the starting microstructure.

The purpose of this investigation was to systematically study, *via* hot compression, the recrystallization behavior of commercial as-cast 316L during hot working. In this study, the compression specimen axis was oriented parallel to the columnar grains to eliminate abnormal deformed-specimen geometries, allowing the development of an accurate kinetic relationship between volume fraction recrystallized and the deformation parameters (ε, $\dot{\varepsilon}$, and T). The role of δ-ferrite in recrystallization is examined. Application of the data to commercial processing is discussed.

II. EXPERIMENTAL PROCEDURE

A. *Materials*

The material studied in this investigation is as-cast 316L austenitic stainless steel supplied by Lukens Inc. (now a subsidiary of Bethlehem Steel Co.). The ingots were bottom poured and cast to dimensions of 0.58-m high × 1-m long × 1-m wide. The chemical composition of the steel is given in Table I.

Table I. Chemical Composition (Mass Percent) of As-Cast 316L

Cr	Ni	Mo	Mn	Cu	Co	Si	Nb
16.8	10.6	2.12	1.71	0.48	0.18	0.46	0.026
Al	Ti	Sn	Pb	C	N	S	P
0.001	0.001	0.0017	0.001	0.016	0.042	0.006	0.027

B. *High-Temperature Compression Testing*

In order to properly locate and orient the compression samples in the columnar grain region of the ingot, a transverse section was cut from the bottom half of the ingot and macroetched.[9] A chill zone, approximately 75-mm thick, composed of coarse equiaxed grains is located at the bottom surface of the ingot. Inside this outer layer is a zone of coarse columnar grains, oriented at right angles to the surface. Cylindrical compression samples were machined from the columnar grain region with specimen axis parallel to the axes of the columnar grains. Compression specimens were 19.05-mm long by 12.70 mm in diameter and had a recessed cavity on each end, with an inner diameter of 2.54 mm, an outer diameter of 12.19 mm, and a depth of 0.127 mm. The cavities were filled with a glass lubricant, Deltaglaze 347 (Acheson Collids Co.), prior to compression testing. The combination of specimen geometry and lubrication effectively eliminates sample barreling to strains greater than one.[10]

Hot compression tests were performed on a 250 KN servohydraulic testing machine (MTS Corp.) outfitted with astrolloy alloy compression rams, silicon nitride compression platens fastened to the ends of the rams, and a three-zone resistance clam-shell furnace. Schematics of the compression specimen geometry and test setup is provided elsewhere.[10] Test samples were loaded onto the bottom die in the furnace and held for 10 minutes prior to deformation. Heating of the specimen was monitored by a thermocouple that was spring-loaded into contact with the specimen. Samples reached the test temperature within about 5 minutes. The velocity of the moving die was varied *via* computer control in order to apply deformation at a constant true $\dot{\varepsilon}$ of 1 s^{-1}. True stress-strain behaviors were determined from the recorded load-displacement data assuming the maintenance of a cylindrical geometry during compression and by correcting the displacement data for load frame compliance. The final specimen height was measured and found to comply with the calculated value.

To simulate production conditions, four temperatures (1000 °C, 1050 °C, 1100 °C, and 1150 °C), strains (0.1, 0.25, 0.5 and 1.0), and postdeformation hold times (2, 36, 360, and 3600 seconds) were investigated. Hold time (t) was applied at the temperature of deformation. The low strain levels represent the degree of deformation imposed during an individual pass, while the higher strain levels simulate the accumulation of strain during multiple passes. Shorter hold times represent interpass dwell times, while the intermediate times are indicative of those times associated with the total time involved in a number of deformation passes. The longest time represents that required to reheat the workpiece in a furnace. A constant $\dot{\varepsilon}$ of 1.0 s^{-1}, which approximates that encountered during most primary breakdown processes, was used in all tests.

C. *Microscopy*

The compressed samples were cross sectioned with a diamond saw so that the face examined in light microscopy contained the compression specimen axis. The cross sections were mounted, polished by conventional techniques, and electrolytically etched with a mixture of 60 mL HNO_3 and 40 mL H_2O at 1.1 V. The volume fraction recrystallized and recrystallized grain size were calculated by point counting. A JEOL* model 840 scanning electron microscope was used to evaluate the elemental composition of the phases in the as-cast microstructure. Transmission electron microscopy (TEM) was used to study the fine structure of both as-cast and hot-worked conditions. Thin foils were produced by cutting 0.4-mm wafers with a slow speed diamond saw to minimize damage. The wafers were then reduced to approximately 0.9 mm by mechanical abrading, punched to 0.3-mm diameter, mechanically abraded to 0.01 mm, and electropolished until perforation in a Fischione (Export, PA) model-110 twin jet polisher, in a 5 vol pct perchloric acid and 95 vol pct acetic acid mixture at 25 V and 30 mA at room temperature. The foils were examined with a PHILIPS* EM 400 transmission electron microscope, operated at 120 kV, and a PHILIPS CM20 scanning transmission electron microscope, operated at 200 kV. Bright-field (BF) and centered dark-field (CDF) imaging were accomplished in addition to selected area electron diffraction (SAD) and energy dispersive X-ray spectrometric microchemical analysis (EDS).

*JEOL is a trademark of Japan Electron Optics ltd. Tokyo.

*PHILIPS is a trademark of Philips Electronic Instruments Corp., Mahwaha, NJ.

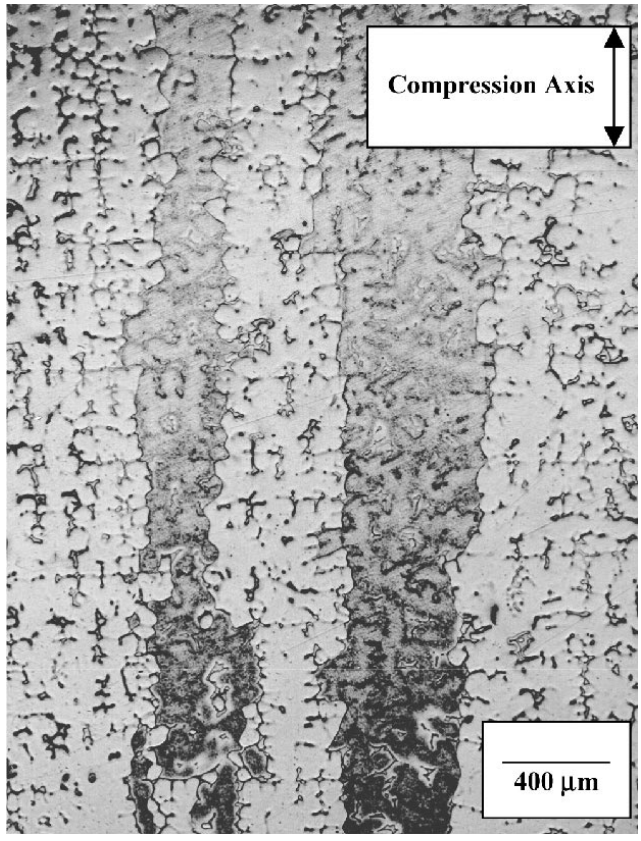

Fig. 1—Columnar grains in as-cast 316L. The axis of the compression specimens is oriented vertically in figure, arrow, parallel to long axis of columnar grains. Light micrograph.

III. RESULTS

A. *Starting As-Cast Materials*

1. *Microstructure*

Figure 1 shows the columnar grain structure of the as-cast 316L. The orientation of the compression specimen axis (arrow in figure) is parallel to the major axes of the columnar grains. Figure 2(a) shows the vermicular (skeletal) morphology of the δ-ferrite (darker phase in the figure) in the as-cast condition. Figure 2(b) shows the faceted nature of the δ that suggests an orientation relationship and a semicoherent interface exists between δ and austenite (γ), discussed further in section III-A-2. The amount of δ in the as-cast state can be calculated from the starting elemental composition using Cr and Ni equivalents, given in Table II, and from diagrams such as that of Delong[11] and the Welding Research Council (WRC (New York, NY)).[12] From these diagrams, the volume percent of δ-ferrite (V_δ) is predicted to be approximately 4.2 and 4.1, respectively. These values are in good agreement with the average value, measured with a Feritscope MP3C (Fischer Co.), of 4.4. The measured V_δ ranged from 3.9 to 5.9.

According to the findings of Brown,[13] Boultbee and Schofield,[14] and Kuo,[15] δ is located along the spines of the dendrites and dendrite arms, consistent with a primary δ solidification mode. Suutula,[16] using the coefficients of Hammer and Svensson[17] (Table II), determined that a Cr_{eq}/Ni_{eq} ratio below 1.5 results in primary austenite followed by ferrite (A/F solidification) and ratios between 1.5 and 2.1 result in primary ferrite with the peritectic or eutectic solidification of austenite (F/A solidification). The WRC-92 ratio for the transition from primary austenite to primary ferrite is 1.4.[12] The corresponding calculated ratios are 1.63 and 1.56, respectively, for the 316L alloy studied here, indicating that 316L will solidify as F/A, consistent with the observed microstructure (Figs. 1 and 2). Equilibrium calculations, performed with Thermo-Calc (Thermo-Calc software AB, Stockholm, Sweden) software also predict the F/A solidification sequence.

Measured values of the spacing between primary and secondary dendrite arms are given in Table III. Recrystallization has been suggested to be a function of the secondary dendrite arm spacing[18] and also a function of the amount of δ-ferrite.[7] The mean free path between delta particles should play a role in deformation, dislocation substructure evolution, and, thus, recrystallization. It was measured to be approximately 85 μm, which is equivalent to the mean free path of an equiaxed grain structure having a nominal grain diameter of approximately 95 μm and is approximately equal to the measured secondary dendrite arm spacing (100 μm, Table III). Assuming nucleation is equally probable along every interphase boundary, recrystallization, at least in the incipient stages, may be proportional to the interphase boundary area (IBA), which can vary, at constant V_δ, with the shape of δ. The IBA per unit volume, calculated by the method of Saltykov,[19] was 43.3 mm^{-1}, which

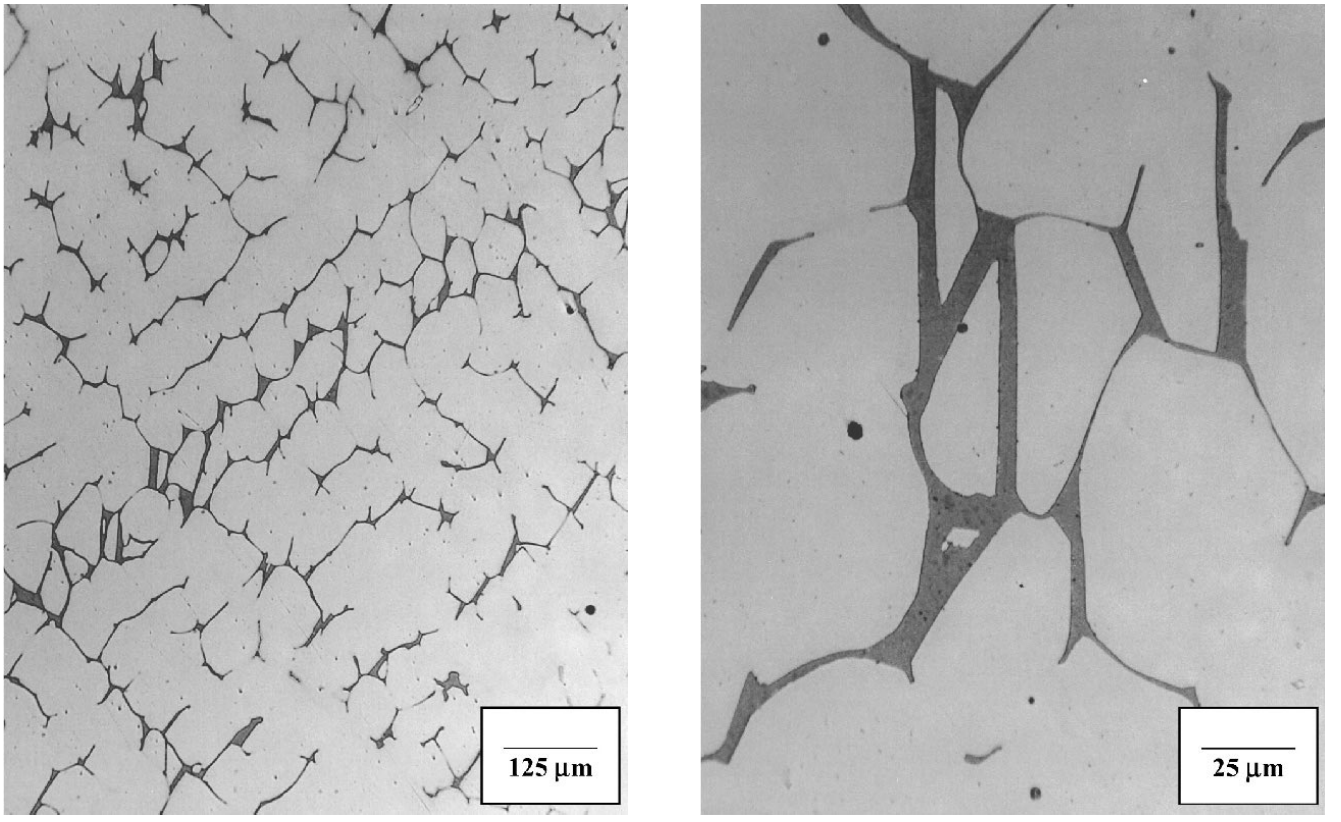

(*a*) (*b*)

Fig. 2—As-cast 316L showing (*a*) vermicular structure of the δ and (*b*) straight sided segments of δ, indicating the existence of an orientation relationship between δ and γ. Light micrographs.

Table II. The Cr and Ni Equivalents, Calculated and Measured Volume Percent δ-Ferrite in As-Cast 316L*

Parameter	Delong	WRC-92	Hammer & Svensson
Cr equivalent	19.623	18.938	20.449
Ni equivalent	13.195	12.120	12.558
Ratio	1.49	1.56	1.63
Prediction	4.2	4.1	F/A
Measured	4.4 (5.0)	4.4 (5.0)	F/A

*Volume percent δ-ferrite was calculated from the Delong diagram[11] (Cr_{eq} = Cr + Mo + 1.5Si + 0.5Cb; Ni_{eq} = Ni + 0.30 (N + C) + 0.5Mn) and the WRC-92 diagram[12] (Cr_{eq} = Cr + Mo + 0.7Nb; Ni_{eq} = Ni + 35C + 20N + 0.25Cu). Ferrite content was measured with a Feritscope model MP3C. Volume percent ferrite (shown in parenthesis) was also calculated by metallographic point-count. Hammer and Svensson equivalents[17] (Cr_{eq} = Cr + 1.37Mo + 1.5Si + 2Nb + 3Ti; Ni_{eq} = Ni + 0.31Mn + 22C + 14.2N + Cu) were used to predict solidification mode. F/A signifies that δ-ferrite precipitates form the melt first, followed by austenite. A/F signifies the opposite sequence.

Table III. As-Cast Dendritic Spacings, Lengths, and Range of Effective Initial Grain Diameter in As-Cast 316L*

Spacing between primary arms	273 μm
Spacing between secondary arms	100 μm
Length of primary arms	>20.0 mm**
Range of effective initial grain diameter	55 to 95 μm

*An effective initial grain diameter of 55 μm was calculated on the basis of the measured interphase boundary area available for the nucleation of recrystallization. The 95 μm value is based on the measured mean free path between delta ferrite particles.

**Primary dendrite arms extended across entire polished surface of length 20.0 mm.

is analogous to the IBA per unit volume for a single-phase equiaxed structure with a grain size of 55 μm (Table III). Thus, the effective initial grain size in the starting material probably has a value that lies between 55 and 95 μm (ASTM 5.5 and 4). Although the calculated range of effective initial grain size is relatively fine and comparable to those typically found in wrought microstructures, the recrystallization rate of the as-cast 316L will be shown to be slower than in equivalent hot-worked (wrought) 316L. The relatively sluggish recrystallization kinetics of the as-cast 316L will be related to the crystallographic texture in the compression samples.

Although present in the as-cast material, δ could dissolve upon reheating for testing (or, similarly, on reheating for primary breakdown of the ingot). To assess the stability of δ, samples of the as-cast material were heated to temperatures between 900 °C and 1300 °C for 1 hour, followed by water quenching. Measurements showed that reheating had no effect on the amount of δ, although some spheroidization did occur at the highest temperature, 1300 °C. As shown later (Figure 10(a)), the morphology of the δ remains relatively unchanged on heating for 1 hour at 1150 °C, the highest temperature tested in this study. Thus, there is little effect of the heating time prior to compression testing on the amount and morphology of the δ.

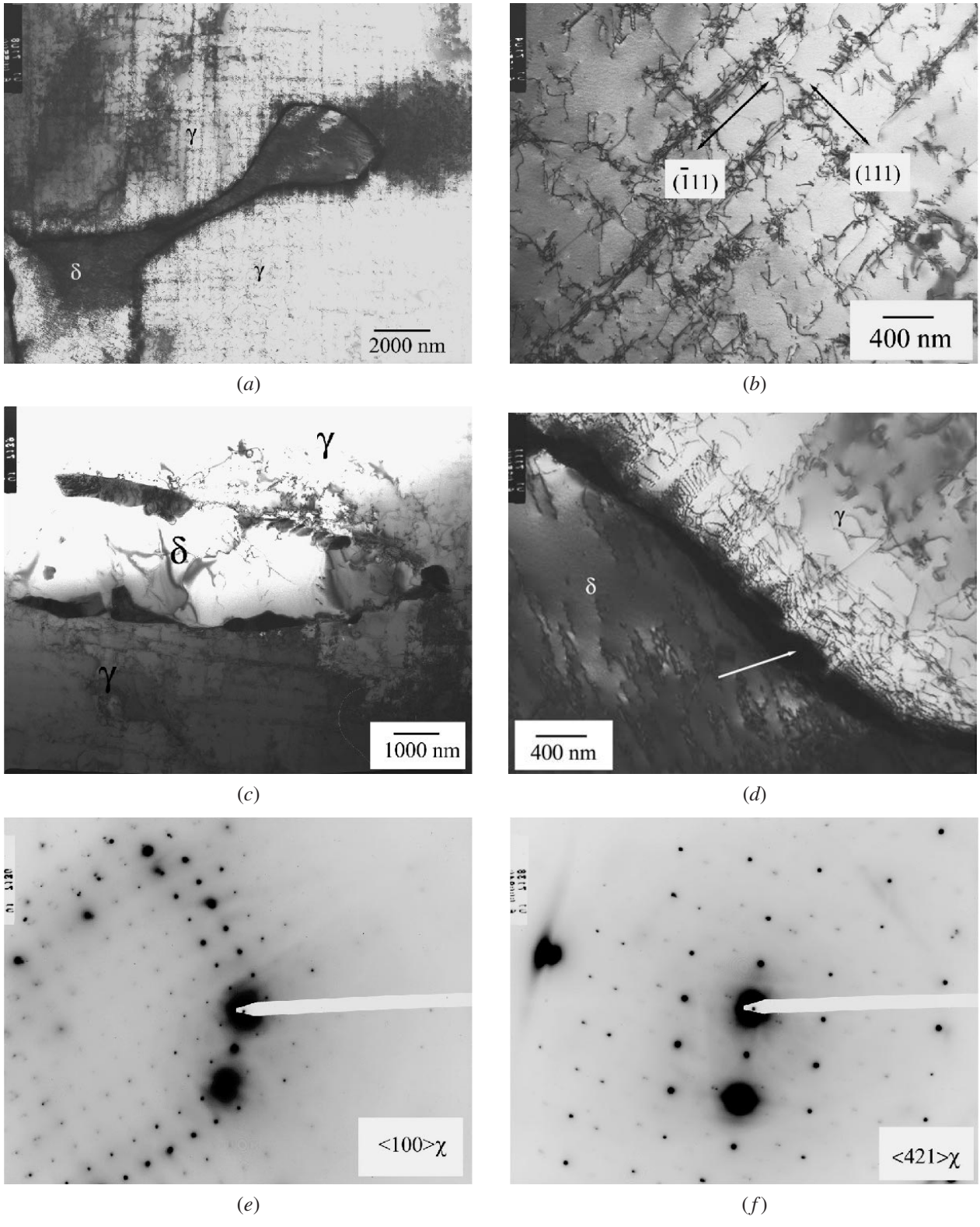

Fig. 3—TEM micrographs and diffraction patterns of as-cast 316L: (*a*) vermicular morphology of δ and dislocation structure in γ and δ, (*b*) planar arrays of dislocation tangles in γ associated with two operative (111) type slip planes, (*c*) precipitates at the γ-δ boundaries, (*d*) dislocations generated at the γ-δ boundary and in association with precipitates, and (*e*) and (*f*) examples of electron diffraction patterns from the precipitates identifying them as χ phase.

2. *Fine structure*

Figure 3 presents TEM observations of the as-cast condition. Figure 3(a) shows that a significant dislocation substructure exists in both γ and δ in the as-cast state. Planar arrays of dislocation tangles are present in the γ. Selected area diffraction (SAD) observations coupled with trace analysis indicate that the planar arrays are associated with intersecting slip planes in the γ (Figure 3(b)). The dislocation tangles are due to

dislocation interactions at the intersection of slip planes. Higher-magnification observations (not shown) reveal that the dislocation substructure in δ is characteristic of deformation in ferrite, clusters of screw-type dislocation dipoles and loops. Individual dislocations are curved and frequently jogged and kinked due to dislocation interactions. Dislocations can be generated during a casting/solidification process by (1) thermal contraction stresses, (2) differential thermal contraction between the δ and γ phases, (3) the solid state $\delta \rightarrow \gamma$ transformation, and (4) precipitation. In the current study, all of the sources of stress cited contributed to generation of the dislocation substructure observed in both phases.

Figure 3(c) shows a semicontinuous distribution of precipitates present at the δ/γ interface. Precipitate morphology could be classified as allotriomorphic and some of the individual precipitates appear to be faceted, indicating a crystallographic relationship exists with one of the abutting phases. Dislocations in δ and γ appear to be generated at the δ/γ interface and, more specifically, in association with the precipitates on the interface (Figure 3(d)). Higher-magnification observations (not shown) of the dislocation substructure in δ close to the interface show that screw dipole dislocations appear to be parallel to the δ/γ interfacial structure on which precipitates have grown.

There are locations in the microstructure at which the δ/γ interface precipitates have coarsened significantly, allowing identification *via* SAD and EDS. Figures 3(e) and (f) are SAD observations that identify the precipitates as χ phase, a body-centered cubic (bcc) structure rich in Cr and Mo and related to the σ and Laves phases that have been observed[20] to form in stainless steels at elevated temperatures. An estimate of the χ-phase lattice parameter, derived from the SAD observations, is 8.90 A, which is close to that cited by Andrews *et al*.[21] Antiphase domain boundaries, a structure produced in ordered materials when like atoms become nearest neighbors,[22] are present in the larger χ particles (evident from symmetrical fringe contrast in the χ phase), indicating that the χ phase, observed to nucleate at δ/γ interfaces in the current work, is ordered, at least in the latter stages of growth.

The EDS analyses of δ, γ, and precipitate regions are summarized in Table IV. The δ and γ phases are enriched and depleted, respectively, in the ferrite-stabilizing elements Cr and Mo. The mean precipitate chemical composition is $Cr_{8.47}Fe_{14.36}Mo_{6.17}$, which is similar to that cited for χ phase by Andrews *et al*.,[21] $Cr_6Fe_{18}Mo_5$.

Although an exhaustive study was not made, SAD observations indicated that a Kurdjumov–Sachs[23] (KS) or Nishayama[24]–Wasserman[25] (NW) crystallographic orientation relationship exists between ferrite and austenite across some δ/γ interfaces, while another orientation relationship, recently described by Headley and Brooks,[26] exists across others. The KS and NW orientation relationships are slightly deviated from one another and basically involve parallelism between close-packed planes and close-packed directions within those planes, in the austenite and ferrite. A KS or NW crystallographic orientation relationship has been observed by workers studying as-cast 316 stainless steel (CF8M) and related to evolution of δ morphology.[27] In the Headley–Brooks (HB) orientation relationship, close-packed planes in the two phases are still parallel, but close-packed directions in these planes are not. The HB relationship is rotated 30 and 35.26 deg from the KS and NW relationships, respectively. Headley and Brooks concluded that the new orientation relationship could coexist with the KS and NW orientation relationships and was associated with a mixed solidification mode in which a large fraction of liquid solidifies as primary δ and the remaining liquid solidifies as γ (F/A solidification). They theorize that the lower strain energy associated with formation of γ during solidification compared to that during solid-state transformation accommodates the evolution of the different crystallographic orientation relationship (HB). The observance of an HB orientation in the material studied here, which also solidifies *via* F/A, as discussed earlier, is consistent with their findings.

Table IV. Elemental Composition of Various Phases (Mass Percent) in As-Cast 316L, Determined with EDS

Feature	Fe	Cr	Ni	Mo	Mn
δ	61.5	25.6	3.86	6.77	2.19
γ	66.8	19.1	8.73	2.54	2.89
Particle	41.8	23.0	2.86	30.8	1.55

The character of the δ/γ interfaces should be important in the accommodation of deformation. Pinol-Juez *et al*.[28] investigated the hot deformation behavior of a duplex stainless steel at 1000 °C at a $\dot{\varepsilon}$ of 1 s^{-1} and showed that extensive grain boundary sliding occurred at the interfaces if they were incoherent, as in wrought structures. Limited sliding occurred on coherent or semicoherent interfaces where a K–S orientation relationship between δ and γ was observed in the as-cast condition. The fact that limited sliding was observed for K–S interfaces, also observed in this study, supports the notion of an "effective" grain size associated with the δ, *i.e*., the δ/γ interfaces do not easily accommodate strain locally and, thus, will be effective in the nucleation of recrystallization. On the other hand, the authors also observed that deformation was accommodated preferentially by shearing of the δ. Local accommodation of strain by δ could preclude the generation of a dense dislocation substructure in γ, near the interface, and thus moderate nucleation events.

B. *Measured Flow Curves*

Figure 4 shows the true stress-strain behavior of as-cast 316L deformed at a $\dot{\varepsilon}$ of 1.0 s^{-1} and at the four temperatures studied (1000 °C, 1050 °C, 1100 °C, and 1150 °C). The flow curves are well behaved, stress increasing monotonically with strain, and show no signs of instability that accompanies abnormal flow in coarse-grained or textured specimens. Likewise, the deformed specimen geometries were cylindrical after deformation, although the effect of the coarse grain structure was observed on the unconstrained surface as a coarse "orange-peel."

Softening in the flow curves, should it occur, is often associated with the onset of dynamic recrystallization. For example, plotted in the figure is an equivalent curve for as-cast columnar 316L tested at 1000 °C at a $\dot{\varepsilon}$ of 1 s^{-1}, developed in torsion by Ryan and McQueen.[8] At strains up to 0.5, the two curves, one developed in compression and the other in torsion, nearly overlap. However, at higher strain, the torsion curve shows that softening ensues at a ε of about

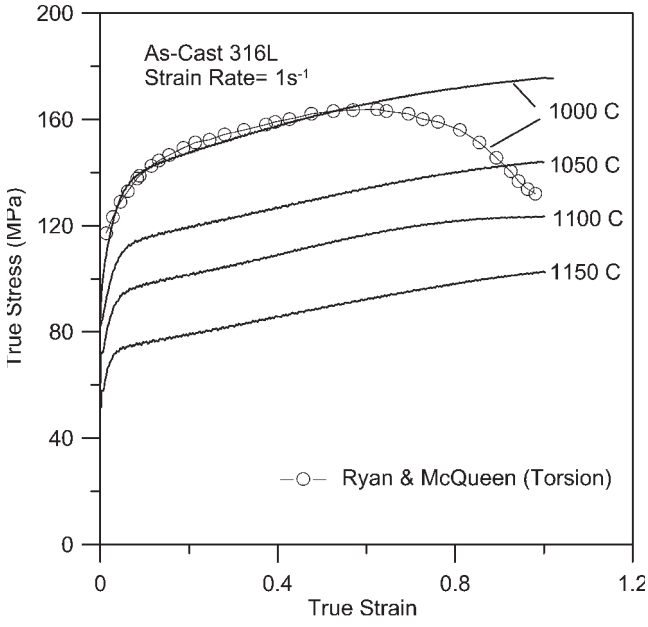

Fig. 4—Flow curves for as-cast 316L stainless steel tested isothermally in compression at a strain rate of 1 s^{-1} at temperatures ranging from 1000 °C to 1150 °C. The axis of the compression specimen was parallel to the primary axes of the columnar grains. Monotonic hardening with strain is observed, indicating that dynamic recrystallization is not operative during deformation. The curve with circle symbols is from Ryan and McQueen[8] for as-continuously-cast 316L tested at a strain rate of 1 s^{-1} at 1000 °C in torsion.

0.6. In that study, softening was interpreted to be due to the onset of dynamic recrystallization. However, no evidence for dynamic recrystallization was encountered in this study. In the same study,[8] the degree of static recrystallization was inferred from the degree of softening observed in the flow curves during torsional interruptions. The degree of static recrystallization inferred for as-cast 316L was much greater than that observed here, as will be shown. A number of studies document differences between fractional softening measured from flow curves and the volume recrystallized measured by microstructural examination. For example, Baraclough and Sellars[29] measured the volume recrystallized and fractional softening in wrought 304L and found that in torsion the fractional softening was not linearly related to fraction recrystallized. The nonlinearity was associated with inhomogeneous deformation and recrystallization in highly deformed regions, and to the subsequent localization of deformation in these "soft" areas upon reloading. As a result, a lower flow stress was measured than if the strain was homogeneously distributed.

Sah *et al.*[30] observed localized flow and recrystallization during the hot torsion of Ni and showed that localized flow resulted in "discs" of recrystallized material, oriented transverse to the gage length, producing a heterogeneous microstructure along the gage length. Other studies of wrought 304L and alloy 718,[31,32,33] deformed repetitively in compression, show that large amounts of softening in the reloaded flow curves are not necessarily related to static recrystallization. For example, alloy 718 deformed at 950 °C shows 50 to 60 pct softening between passes but no recrystallization. At 1050 °C, 50 pct softening corresponds to 11 pct recrystallization. Conversely, at 1150 °C, interpass hold times resulted in significant recrystallization but little softening, presumably due to an aging effect. Thus, it is apparent that a determination of the recrystallization kinetics as well as the role of δ in recrystallization in as-cast stainless steels cannot be obtained from single-pass or multiple-pass flow curves but instead requires a detailed microstructural examination of the hot-worked conditions, such as that presented in Section III-C.

C. *Structural Evolution*

1. *Microstructure*

Figure 5 depicts the progression of recrystallization with time for as-cast 316L deformed to a ε of 0.5 at 1050 °C. Recrystallization nuclei form preferentially at the γ/δ boundaries within 2 seconds after deformation (Figure 5(a)). Some nucleation was also observed at the γ/γ grain boundaries (not shown). The ubiquitous nature of the γ/δ boundaries makes this site for nucleation the more important of the two. Figures 5(b) through (d) show additional nucleation and grain growth with increasing time, 36 to 3600 seconds. In Figs. (c) and (d), the δ appears to have a pinning effect on the newly recrystallized grain boundaries. In fact, it was generally observed that the recrystallized grain size varies with the local spacing of the δ. Even after 3600 seconds at 1050 °C (Figure 5(d)), the recrystallized grain size remained fine (35 μm, corresponding to an ASTM grain size of about 6.5). Also evident in Figure 5 is the progressive spheroidization and dissolution of δ with time, shown in more detail in section III-D.

Figure 6(a) shows an isolated patch of exceptionally large recrystallized grains (approximately 130 μm), which was observed after a ε of 0.1 at 1050 °C and a 3600 s hold. A few large grained patches were also observed at 1100 °C and 1150 °C after equivalent strain and hold time. The process by which a few grains grow excessively after small strains, 0.1 or less, is commonly referred to as abnormal grain growth. Figure 6(b) shows that recrystallization nuclei observed in the three conditions are small twins in the γ that nucleated at γ/δ boundaries. The straight boundaries of the twins are parallel to some of the facets on the δ, suggesting a cooperative mechanism for nucleation involving the three areas (γ-matrix, γ-twin, and δ). The fine twin nuclei were not observed in conditions strained to levels greater than 0.1. Jones[34] observed a similar type of nucleation in copper alloys and stainless steels and Huber and Hatherly[35] referred to the twins as "recovery-twins" to distinquish them from those that form during grain growth. Apparently, these nuclei grow *via* strain-induced boundary migration of the incoherent twin front, which explains the blocky morphology of the large recrystallized grains. Another feature, observed in material deformed to a ε of 0.1, was the migration of the γ/γ dendrite boundaries. This feature was fairly rare and did not dominate microstructural evolution.

Summarizing, recrystallization in 316L begins preferentially at the γ/δ boundaries, which are prevalent in the as-cast microstructures. Recrystallization progresses until the original as-cast coarse columnar structure is replaced by a relatively fine equiaxed recrystallized microstructure. The recrystallized grain size typically varies with the local spacing of the δ, because of the pinning effect of the ferrite. Local areas are found where the grain size and δ-spacing are 3 to 4 times the reported averages.

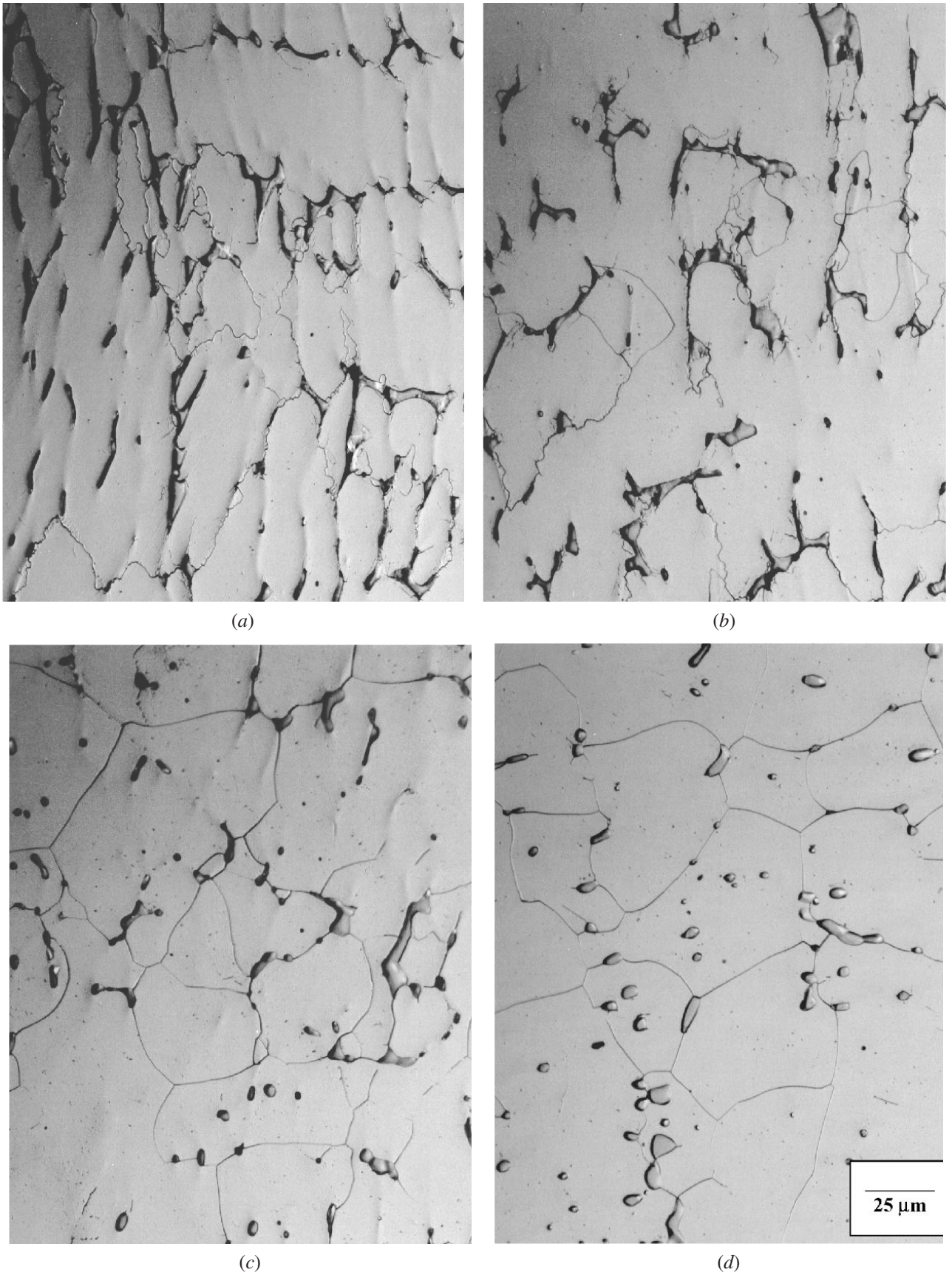

Fig. 5—Recrystallization after $\varepsilon = 0.5$ at 1050 °C for a hold time of (*a*) 2 s, (*b*) 36 s, (*c*) 360 s, and (*d*) 3600 s. Note in (*a*) the recrystallization nuclei at δ (*a*) through (*d*) spheroidization of δ with time, and (*c*) and (*d*) apparent pinning of the recrystallized grain boundaries by δ. The compression axis has a horizontal orientation in photographs. Light micrographs.

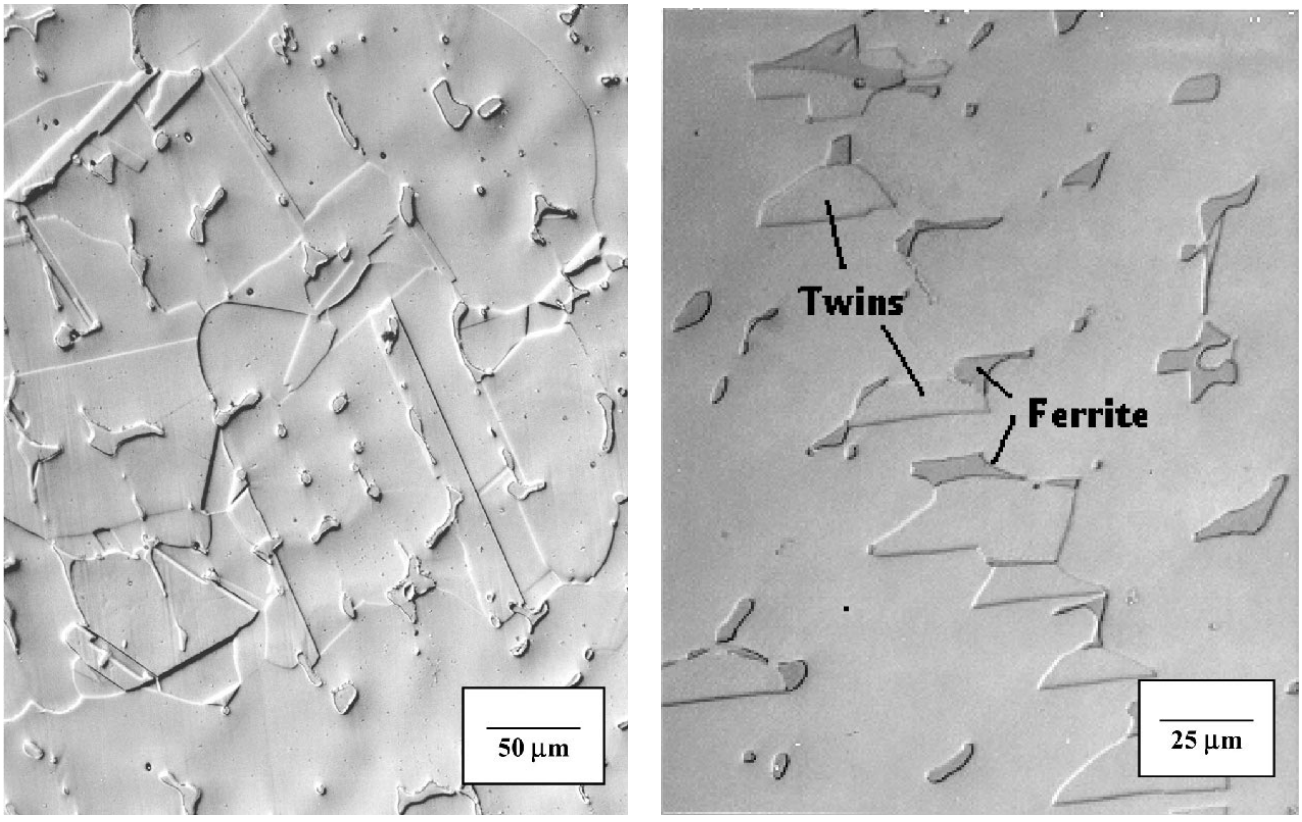

(*a*) (*b*)

Fig. 6—Light microscopy of a sample, deformed to $\varepsilon = 0.1$ at 1050 °C and held for 3600 s, showing (*a*) a patch of large recrystallized grains with straight-sided annealing twins and (*b*) fine recrystallized γ grains, which appear to have a twin orientation with the unrecrystallized γ matrix and which nucleated at δ-ferrite.

2. *Fine structure*

Figure 7 shows the fine structure of selected hot-worked conditions. After a ε of 0.1 at 1000 °C and 2 seconds, the δ is well recovered *via* polygonization (Figure 7(a)). The γ exhibits the initial stages of subgrain formation in the region immediately adjacent to the δ (Figure 7(b)). The arrows in (b) show elongated subgrains with boundaries composed of loosely knit dislocations. Subgrain formation was not observed in the γ matrix away from the δ. With more strain and time, 1.0 and 36 seconds, at 1000 °C, a relatively well-developed subgrain structure forms in the matrix (Figure 7(c)). Recrystallization nuclei form statically and preferentially at the γ/δ interfaces (Figure 7(d)) shown previously *via* light microscopy (Figures 5(a) and (b)). The recrystallization nucleus in (d) appears to be derived from the surrounding subgrain structure by subgrain coalescence or subgrain boundary migration. Highly mobile high-angle boundaries (shown by the inclined boundary fringe contrast) have formed between the nucleus and the surrounding recovered substructure. The nuclei and subgrains appear to have grown into the δ, apparently consuming some of it, which is consistent with the measured reduction in the volume fraction of δ that occurs with time at temperature, discussed further in a later section. After a ε of 0.1 at 1050 °C and during a 3600 seconds hold, a substructure of incipient subgrains formed adjacent to the δ (Figure 7(e)), while a low dislocation density with a random distribution formed in the matrix away from the interphase boundaries (Figure 7(f)). Thus, a ε of 0.1 does not generally introduce enough internal energy to drive recrystallization at temperatures of 1050 °C and below.

The χ phase, present in the as-cast structure, was not observed in any of the hot-worked microstructures. An equilibrium calculation, performed with the computational software TCW@ and thermodynamic database TCFE@ (both from Thermo-Calc Software AB) predicts that χ is unstable above 900 °C. Chi must have precipitated during relatively slow cooling of the casting and dissolved upon subsequent heating and deformation during the compression test cycle. Because χ was not observed after the lowest applied strain (0.1) at the lowest temperature (1000 °C) and the shortest hold time (2 seconds), it apparently has little or no effect on recrystallization, in this study.

3. *Volume recrystallized*

Figures 8(a) though (d) show the variation of V_{REX} with t for the range of parameters studied. The measured values of V_{REX} and the recrystallized grain size, D_{REX}, are provided in Table V. Generally, for each alloy, V_{REX} increases with ε, t, and T, as expected. For example, in samples deformed to a ε of 0.1, little recrystallization is observed until T is increased to 1100 °C and t to 3600 seconds, after which $V_{REX} = 15$ pct. As strain is increased, recrystallization occurs at progressively lower T and t. For example, after a ε of 0.25 and 3600 seconds, significant recrystallization, 26 pct,

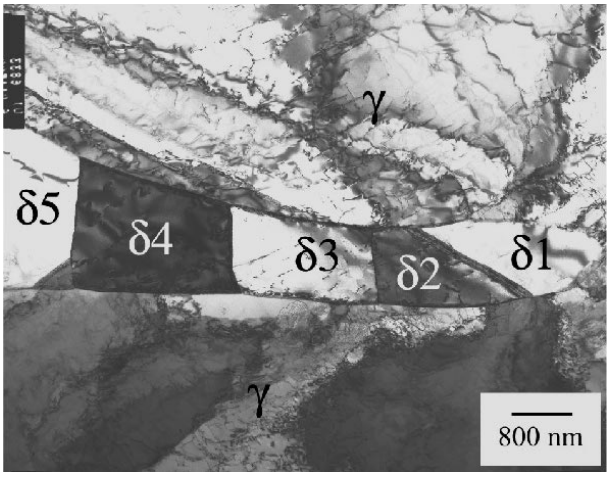

(*a*)

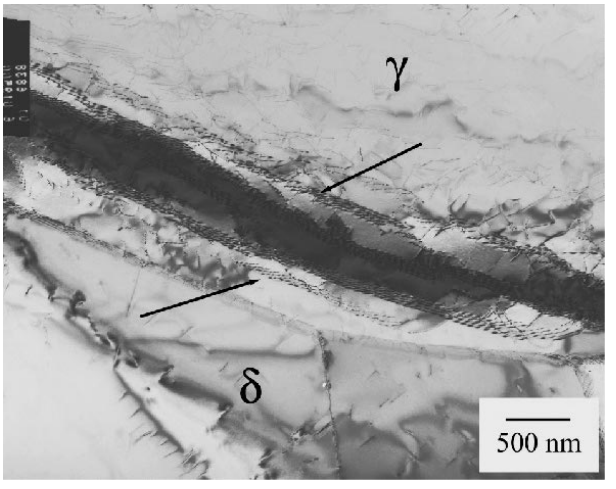

(*b*)

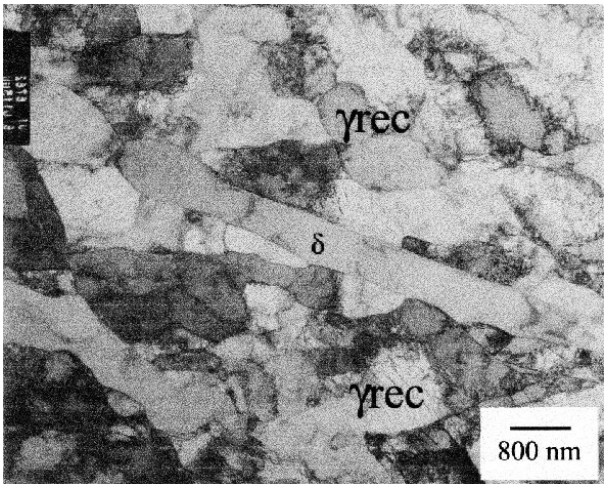

(*c*)

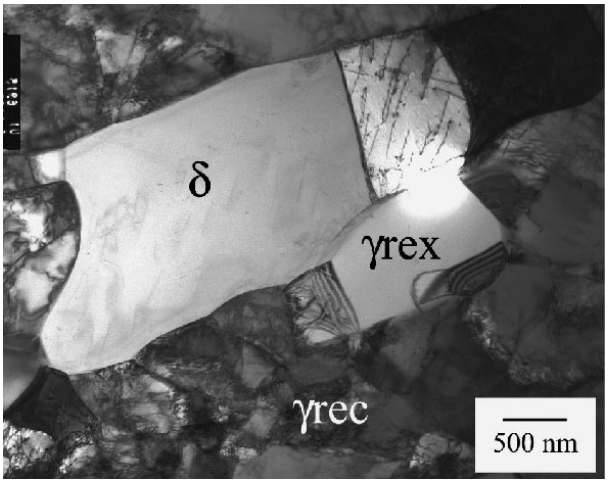

(*d*)

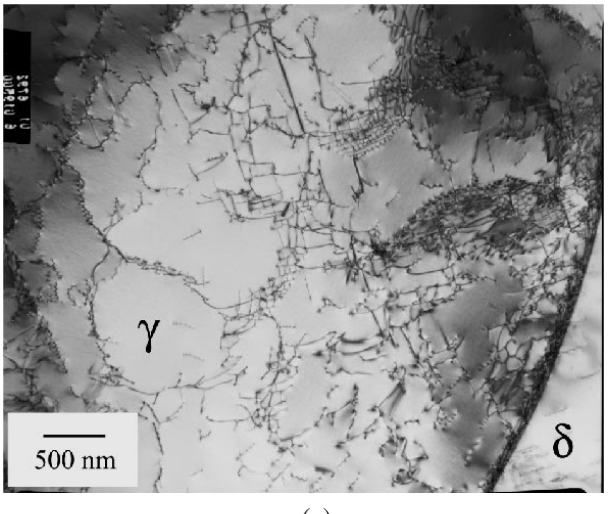

(*e*)

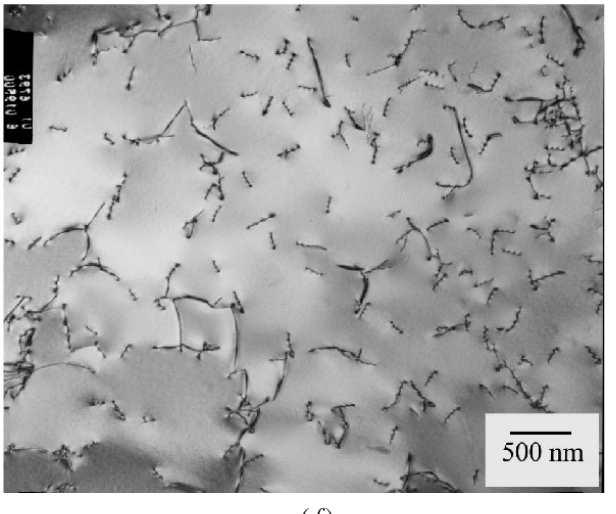

(*f*)

Fig. 7—TEM bright-field micrographs of as-cast 316L after compression at 1 s^{-1} to (*a*) and (*b*) $\varepsilon = 0.1$ at 1000 °C and 2 s hold, (*c*) and (*d*) $\varepsilon = 1$ at 1000 °C and 36 s, (*e*) and (*f*) $\varepsilon = 0.1$ at 1050 °C and 3600 s: (a) segmented δ with orientation differences between each of 1.5 to 2.5 deg, (b) elongated subgrains in γ adjacent to δ in (a), (c) recovered substructure in γ adjacent to δ, (d) recrystallization nuclei which formed at the γ-δ boundary, (e) incipient subgrain structure in γ adjacent to δ, and (f) loose dislocation structure in γ matrix away from the δ in (e).

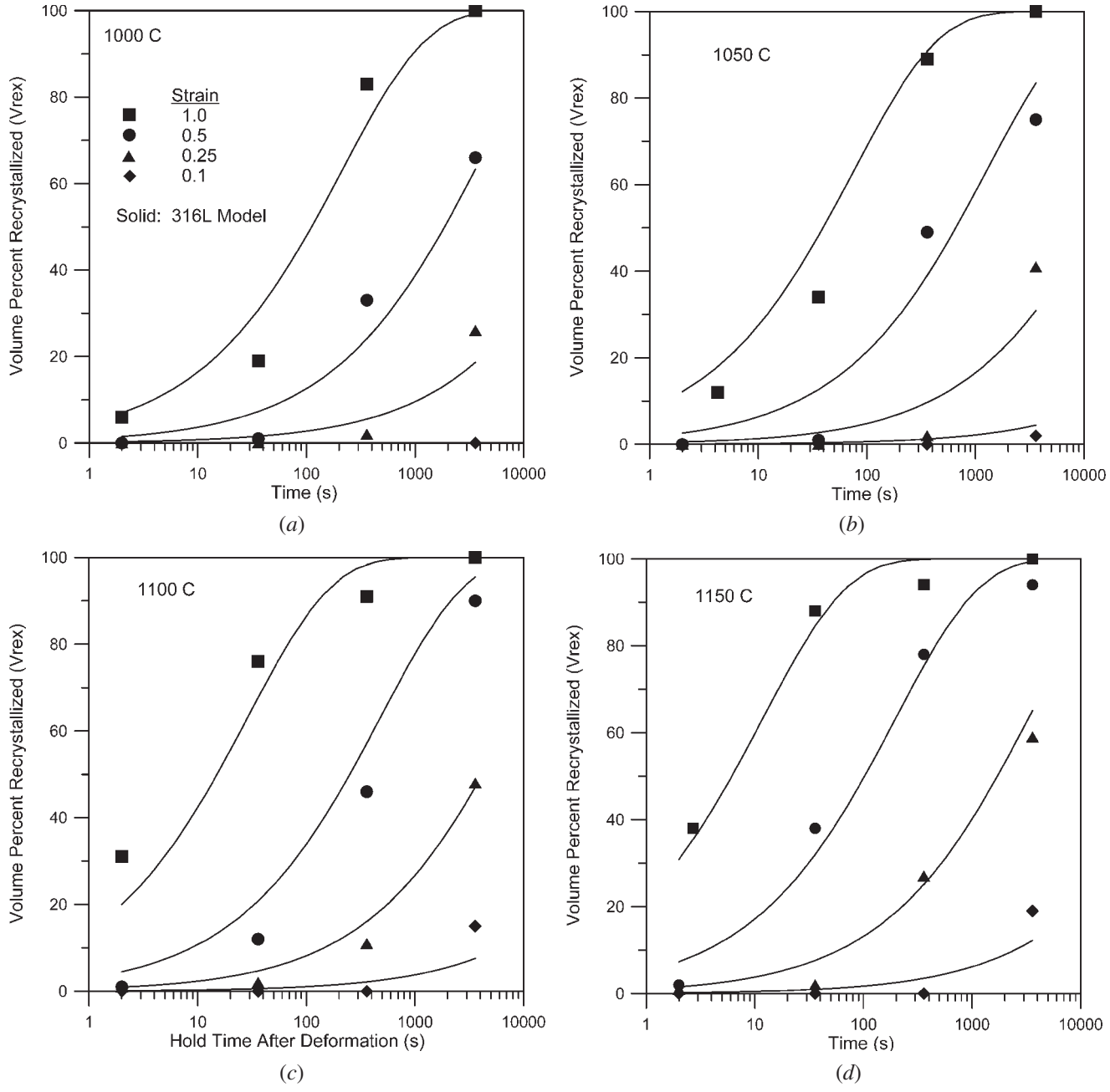

Fig. 8—Variation in percent volume recrystallized, V_{REX}, with hold time at temperature after deformation for strains of 0.1, 0.25, 0.5, and 1.0 at deformation temperatures of (*a*) 1000 °C, (*b*) 1050 °C, (*c*) 1100 °C, and (*d*) 1150 °C. The curves are calculated with Eq. [6] and the best-fit coefficients from Table VI. Measured values from Table V are indicated with symbols.

occurs even at the lowest T employed in this investigation, 1000 °C. At 1000 °C, as strain is increased to 1.0, significant recrystallization occurs at shorter times. For example, $V_{REX} = 83$ and 19 pct after 360 and 36 seconds, respectively.

Evolution of V_{REX} was mathematically modeled for the entire range of testing conditions. The progress of isothermal recrystallization is often described by the following:

$$X_v = 1 - \exp(-Bt^n) \quad [1]$$

where X_v is the volume fraction recrystallized, t is time, and B and n are constants.[36]

Equation [1] relates X_v to the hot deformation variables of ε, $\dot{\varepsilon}$, deformation temperature (T_{DEF}), and annealing temperature (T_{ANNEAL}) through parameter B. It has been shown[37] that the parameter B varies as a function of deformation conditions, annealing temperature, and the Zener–Hollomon parameter (Z) as follows:

$$B = C_1 D_0^{C_4} Z^{C_3} \varepsilon^{C_2} \exp\left(\frac{Q_{RXN}}{RT_{ANNEAL}}\right) \quad [2]$$

Table V. Volume Fraction Recrystallized, V_{REX}, and Recrystallized Grain Diameter (μm), D_{REX}, for As-Cast 316L after Hot Compression to a Strain That Ranged between 0.1 and 1.0; Hold Time, Applied Immediately after Deformation and at the Deformation Temperature, Ranged between 2 and 3600 Seconds

316L	2 s		36 s		360 s		3600 s	
	V_{REX}	(D_{REX})	V_{REX}	(D_{REX})	V_{REX}	(D_{REX})	V_{REX}	(D_{REX})
1000 °C								
0.1	0	(—)	0	(—)	0	(—)	0	(—)
0.25	0	(—)	0	(—)	2	(29)	26	(45)
0.5	0	(—)	<1	(10)	33	(25)	66	(32)
1.0	6	(10)	19	(12)	83	(23)	100	(31)
1050 °C								
0.1	0	(—)	0	(—)	0	(—)	2	(132)
0.25	0	(—)	0	(—)	2	(25)	41	(62)
0.5	<1	(8)	<1	(17)	49	(28)	75	(35)
1.0	12	(13)	34	(17)	89	(26)	100	(32)
1100 °C								
0.1	0	(—)	0	(—)	0	(—)	15	(174)
0.25	<1	(20)	2	(28)	11	(38)	48	(72)
0.5	<1	(18)	12	(23)	46	(30)	90	(38)
1.0	31	(15)	76	(23)	91	(28)	100	(35)
1150 °C								
0.1	0	(—)	0	(—)	0	(—)	19	(155)
0.25	<1	(23)	2	(32)	27	(57)	59	(90)
0.5	2	(20)	38	(28)	78	(45)	94	(49)
1.0	38	(16)	88	(30)	94	(37)	100	(39)

Table VI. As-Cast 316L Recrystallization Model Parameter Values and Goodness of Fit

Fit Parameters	316L
C_1	249,760
C_2	2.2797
E	−163,436
n	0.56139
Goodness of fit (R-squared)	0.9879

where

$$Z = \dot{\varepsilon}\exp\left(\frac{Q_{DEF}}{RT_{DEF}}\right) \quad [3]$$

and where C_1, C_2, C_3, and C_4 are constants; Q_{RXN} and Q_{DEF} are the apparent activation energies for recrystallization and deformation, respectively; and R is the gas constant and is equal to 8.314 J/K/mole. The value of D_o is constant in this study and can be convolved into C_1. Substituting Eq. [3] into Eq. [2] results in the following:

$$B = C_1\dot{\varepsilon}^{C_3}\varepsilon^{C_2}\left[\exp\left(\frac{Q_{DEF}}{RT_{DEF}}\right)\right]^{C_3}\exp\left(\frac{Q_{RXN}}{RT_{ANNEAL}}\right) \quad [4]$$

where T_{DEF} and T_{ANNEAL} are equal in this investigation, allowing simplification as follows:

$$B = C_1\dot{\varepsilon}^{C_3}\ \varepsilon^{C_2}\exp\left(\frac{C_3Q_{DEF} + Q_{RXN}}{RT}\right) \quad [5]$$

By combining C_3, Q_{REX}, and Q_{DEF} into a single energy parameter, E, the form of Eq. [1] becomes

$$X_v = 1 - \exp\left[\left(-C_1\dot{\varepsilon}^{C_3}\ \varepsilon^{C_2}\exp\left(\frac{E}{RT}\right)\right)t^n\right] \quad [6]$$

Optimum values for C_1, C_2, E, and n, determined by least-squares fitting of Eq. [6] to the data in Table V, are given in Table VI. A value for C_3 could not be determined because only one strain rate was used in this study; however, because strain rate equals 1, C_3 need not be determined to apply Eq. [6]. The curves in Figure 8 are calculated with Eq. [6] and the fitted parameters. The Avrami exponent, n, has a value of 0.56, which is within the reported range (0.5 to 1.5) for alloy 304L.[38,39] Typically, the exponent decreases with increasing heterogeneity of recrystallization. Barraclough and Sellars[29] showed that in 304L, n decreases with increasing grain size and attributed the decrease to microscopically local concentration of the deformation followed by locally accelerated recrystallization and then subsequent slower growth into areas of lower local strain. Towle and Gladman[38] attributed a decrease in recrystallization rate with time in 304L, and lower n values, to concurrent recovery of the dislocation substructure in the unrecrystallized matrix as recrystallization proceeds. Both explanations could account for the relatively low n value here, since recrystallization starts locally at delta ferrite islands where the dislocation density is high (Figures 7(a) through (e)) and continues by growing into the adjacent matrix of lower dislocation density (Figure 7(f)). Also, the anticipated higher SFE of 316L would favor more rapid recovery, compared to 304L, and a smaller value of n. Another potential factor could be the ongoing spheroidization and dissolution δ, which may render incipient recrystallization nuclei impotent.

4. *Recrystallized grain size*

The size of the recrystallized grains was measured during the transient stages of recrystallization and, for the purpose of this study, will be referred to as the transient recrystallized grain size, D_{TRAN}, distinquishing it from the typically reported recrystallized grain size, which is measured after recrystallization is complete, commonly referred to as D_{REX}. Interest in D_{TRAN} arises because subsequent rounds of recrystallization of the initially recrystallized material may occur prior to completion of the first wave of recrystallization and the associated kinetics will depend on D_{TRAN}.[33] Repeated recrystallization allows the maintenance of a fine grain size during multiple step hot working processes. Generally, D_{REX} increases with temperature and initial grain size and decreases with strain. Initial grain size was not varied in this study but similar dependencies of D_{TRAN} on temperature and strain are evident in Figure 9. Figure 9 also shows that D_{TRAN} increases as recrystallization progresses, but with greater applied strain, 0.5 to 1, D_{TRAN} is maintained at a relatively fine level. For example, after a ε of 1 (solid curves at bottom in figure), D_{TRAN} increases from about 10 μm at the incipient stages of recrystallization to about 35 μm as recrystallization is completed. After a ε of 0.5, D_{TRAN} increases from about 20 to 40 μm. As strain decreases further, D_{TRAN} increases more dramatically as recrystallization progresses. For example, after a ε of 0.25, the recrystallized grain size at the start of recrystallization is about 20 to 30 μm, and by 50 pct recrystallization, it increases to about 80 μm. After a ε of 0.1, D_{TRAN} at the start of recrystallization is extremely large, having values ranging from 130 to 175 μm, as shown previously in Figure 6. Summarizing, with the application of greater strain, D_{TRAN} can be maintained at a relatively fine level as recrystallization progresses, yielding a fine D_{REX} after recrystallization is complete and also promoting a subsequent round(s) of recrystallization of that fraction of the as-cast microstructure that recrystallizes initially during conventional multiple step hot working processes.

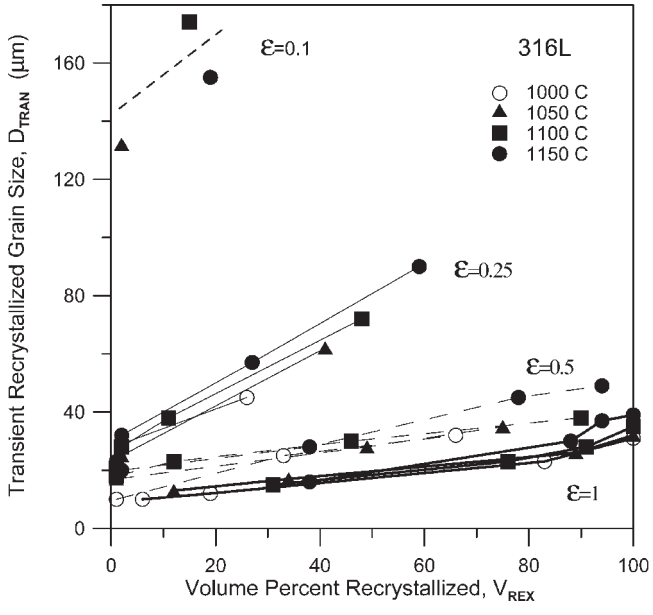

Fig. 9—The variation in transient recrystallized grain diameter, D_{TRAN}, with volume recrystallized (in percent), V_{REX}, for the various applied strains and temperatures investigated.

D. *Spheroidization and Dissolution of Delta-Ferrite*

Figure 5 demonstrated that δ plays a prime role in the recrystallization of as-cast 316L. Figure 10 shows that δ evolves in morphology and decreases in amount during the hot working process. Annealing the as-cast condition for 1 hour at 1150 °C does not significantly affect the morphology nor amount of δ (Figure 10(a)). In contrast, a ε of 1 at 1150 °C followed by a 2 second hold causes the δ particle thickness and spacing to be reduced parallel to the compression axis and elongated normal to the compression axis (Figure 10(b)). The vermicular morphology is still evident. Approximately 9 pct of the δ dissolved and 38 pct of the structure recrystallized (grain boundaries not revealed by etching procedure). With a t of 3600 seconds, after the same deformation, 88 pct of the δ dissolved and substantial spheroidization of the δ occurred. Although not evident, the γ is completely recrystallized (Table V). Even with a low ε of 0.1 at 1150 °C, there is still significant dissolution (41 pct) and spheroidization of δ during a 3600 second hold. In this case, little recrystallization (19 pct) was observed.

Measurements of the extent of dissolution of δ with time at temperature are summarized in Figure 11. Also shown are the concomitant data for V_{REX}, from Table V. Figure 11(a) shows that the degree of dissolution after an applied ε of 0.1 increases with time while the extent of recrystallization lags. Note that about 20 pct dissolution occurred at 360 seconds without recrystallization. The scatter in the data is due to the fact that the amount of δ varies with position in the as-cast structure and that measurements prior to deformation and after deformation were not made in exactly the same locations. Figure 11(b) shows the effects after an applied ε of 1. A comparison of Figure 11(a) to (b) shows that there is little effect of strain on the rate of dissolution, up to 360 seconds. For both strain levels, the level of dissolution at 360 seconds is in the 20 pct range. However, recrystallization increases dramatically, from zero to about 90 pct, as strain is increased from 0.1 to 1. The wide variation in recrystallization and little variation in dissolution between the two levels of strain suggest that the process of recrystallization itself does not enhance dissolution, nor does the increase in strain from 0.1 to 1. A minimum level of strain is required, however, because the sample heated to 1150 °C for 3600 seconds without prior straining did not exhibit any dissolution (Figure 10(a)). Thus, it appears that dissolution is enhanced by the subgrain structure that forms in the γ adjacent to δ or by modification of the δ/γ interface structure, even after the lowest strain. There is a rapid increase in the rate of δ dissolution from 360 to 3600 seconds (Figure 11(b)), which may be related to the newly recrystallized structure in that the many new γ-γ grain boundaries should accommodate the diffusion of the substitutional alloying elements that stabilize δ and γ. The lack of dissolution during the early stages of recrystallization, up to 360 seconds, may be due to the fact that during this stage of recrystallization, the new grain boundaries are moving too rapidly to accommodate much diffusion.

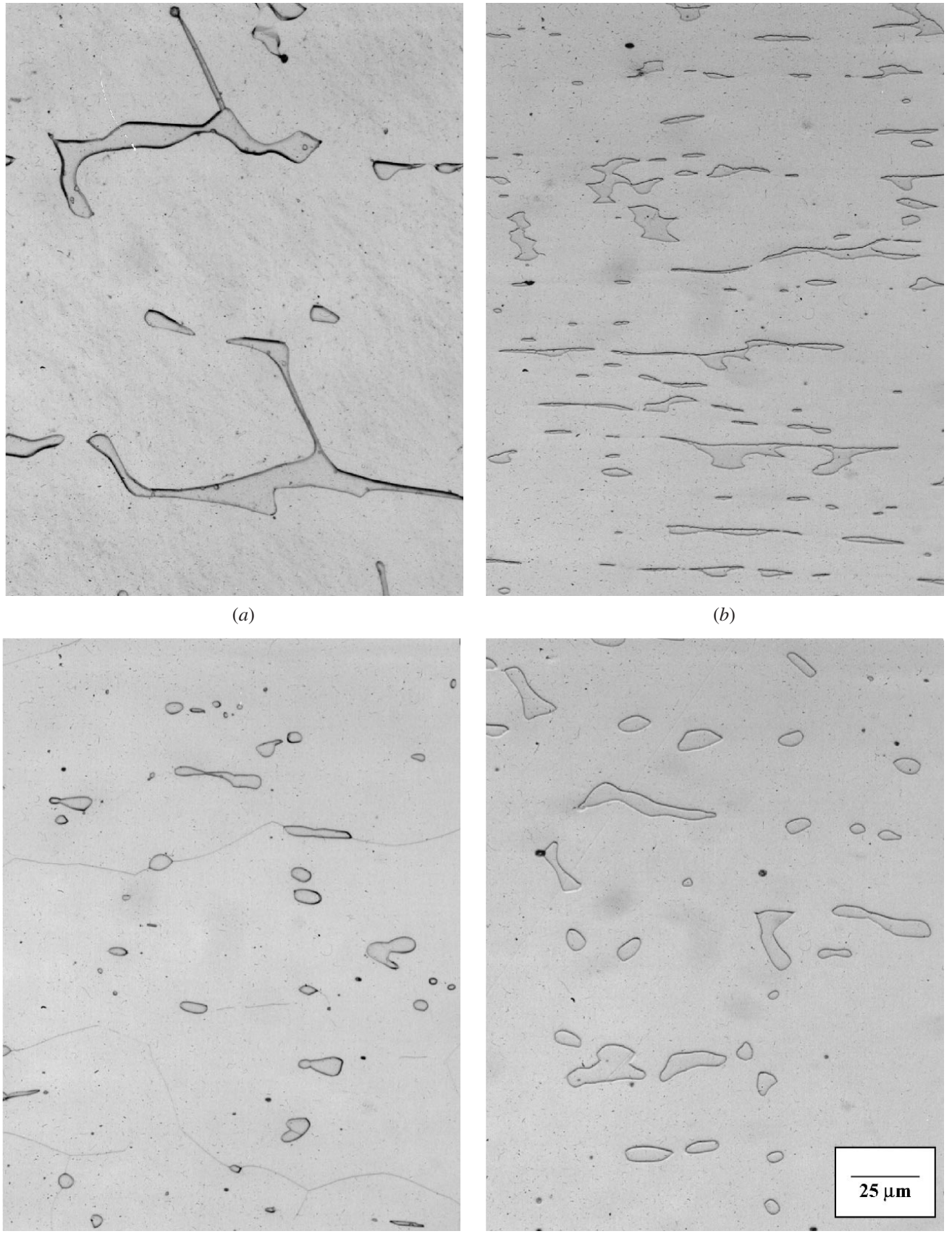

Fig. 10—Light microscopy showing evolution of δ at 1150 °C after (*a*) $\varepsilon = 0$, 3600 s; (*b*) $\varepsilon = 1$, 2 s; (*c*) $\varepsilon = 1$, 3600 s; and (*d*) $\varepsilon = 0.1$, 3600 s.

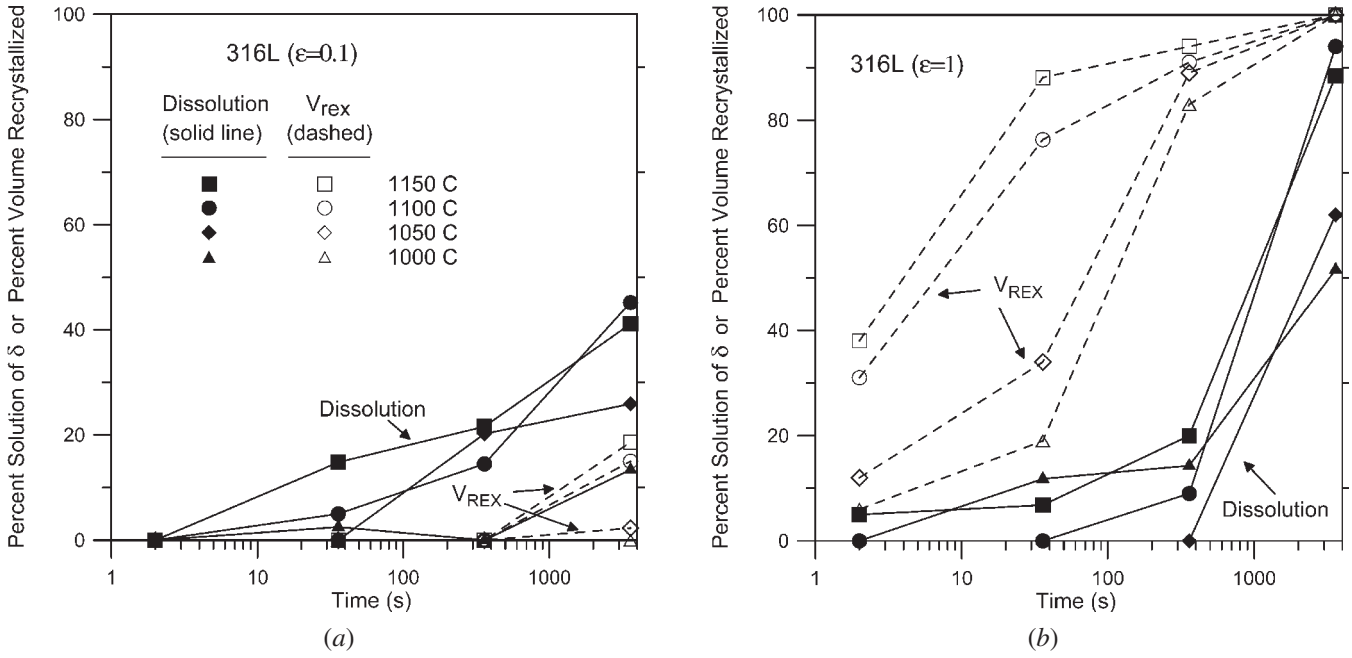

Fig. 11—The variation in percent dissolution of δ and percent volume recrystallized, V_{REX}, with time for temperatures ranging from 1000 °C to 1150 °C and for (*a*) an applied ε of 0.1 and (*b*) a ε of 1.0.

IV. DISCUSSION

A. *Microstructural Behavior*

As shown in Figure 8 and by Eq. [6], the static recrystallization kinetics of as-cast 316L studied here is controlled by various factors that include ε, t, and T. Also, the involvement of delta ferrite in the recrystallization process is demonstrated in the microscopy provided in Figures 5 through 7. Although the initial grain size and strain rate were not varied in this study, they would certainly have a sizeable impact on recrystallization kinetics and grain size evolution. Differences in recrystallization behavior between steels that have undergone identical thermal-mechanical treatment are generally attributed to differences in chemical composition, SFE (determined by composition), secondary phases, and grain size. All of these factors determine dislocation substructure evolution and stored energy of deformation by affecting the rate of dislocation accumulation, the ultimate magnitude of dislocation density, and the microscopic distribution or inhomogeneity of the substructure. For example, Humphreys and Hatherly[40] demonstrated that low SFE values result in an increase in stored energy and dislocation density and related lower SFE to an increased propensity for recrystallization.

Campbell *et al.*[6] and Ahlblom[41] studied the recrystallization kinetics of as-cast 304L after hot compression of coarse columnar grain structures, oriented 90 deg to the compression axis (a soft orientation). The time to 80 pct recrystallization, after a ε of about 0.27 at 1100 °C, in the two studies, was very similar, approximately 600 and 450 seconds, respectively. For similar deformation conditions in this study (Figure 8(c)), the corresponding time for as-cast 316L would be significantly greater, on the order of 10^4 s. The slower recrystallization rate of as-cast 316L is consistent with its higher SFE, calculated[42] to be approximately 50 mJ/m^2, from Table I, *vs* 25 mJ/m^2 for the as-cast 304L. In both studies,[6,41] the recrystallization rate of as-cast 304L material was compared to that of worked and recrystallized material derived from the original casting. For a wrought grain size of approximately 350 μm[6,41], the time to 80 pct recrystallization was reduced by more than an order of magnitude, from 600 to 5 seconds and from 450 to 20 seconds, respectively. The increase in recrystallization kinetics was attributed to the smaller initial grain size in the wrought materials.[6,41]

In order to make a like-comparison in this work, a wrought 316L material (elemental composition given in Table VII), having recrystallized grains sizes of 28 and 286 μm after annealing (Table VIII), was introduced into this study. The two wrought conditions were deformed at 1050 °C to a ε of 1 at a $\dot{\varepsilon}$ of 1 s^{-1} and held for various times. Figure 12(a) shows the variation in V_{REX} with time for the two wrought 316L conditions and the as-cast 316L. The time for 50 pct recrystallization, t_{50}, was 70 seconds for as-cast 316L *vs* 4 and 22 seconds for the fine and coarse grain wrought 316L. However, since the as-cast material is assumed to have an effective grain size in the range 55 to 95 μm, which is intermediate to the two wrought grain sizes, 28 and 286 μm, the t_{50} would be expected to be between 4 and 22 seconds, on the order of 10 seconds instead of 70 seconds. The wrought material has a higher calculated SFE, 65.5 mJ/m^2 (Table VIII), compared to that of the as-cast material, 50 mJ/m^2, which would tend to enhance recovery and slow recrystallization relative to the as-cast material. Thus, the difference in recrystallization kinetics of the two materials is not related to differences in SFE. The wrought

Table VII. Elemental Compositions (Mass Percent) of Wrought Austenitic Stainless Steels Introduced into the Study of As-Cast 316L

	304L	304N	316L	21-6-9	21-6-9	22-13-5	A-286	903
Cr	18.6	18.3	18.0	19.7	19.9	22.2	14.7	—
Ni	10.0	8.1	12.9	6.8	6.7	12.3	30.5	38
Mo	0.055	0.4	2.0	—	—	2.27	1.3	—
Mn	1.9	1.65	2.3	9.5	9.5	5.08	0.03	—
C	0.022	0.053	0.024	0.035	0.029	0.044	0.016	—
Nb	—	—	—	—	—	0.25	—	3
Cu	—	—	0.069	—	—	—	—	—
Al	—	—	—	0.019	0.01	—	0.22	0.7
Ti	—	—	—	—	—	—	2.02	1.4
N	0.015	0.219	0.046	0.31	0.22	0.348	0.0075	—
S	0.0003	0.027	0.003	0.001	0.001	0.009	0.003	—
V	—	—	—	—	—	0.21	0.21	—
P	0.011	0.02	0.013	0.013	0.011	—	0.01	—
Si	0.57	0.72	0.69	0.58	0.53	—	0.07	—
B	—	—	—	—	—	—	10 ppm	—
Co	—	0.11	—	—	—	—	—	15
O	—	—	0.0022	0.0017	0.0013	—	7 ppm	—

Table VIII. Properties of Wrought Austenitic Stainless Steels Introduced into the Study of As-Cast 316L**

	304L			304N		316L		21-6-9		21-6-9		22-13-5		A-286		903
D_0	38	250	512	53	108	28	286	85	112	85	128	20	150	41	203	293
σ (1150 °C)	83	79		110	108	110	95	114	113	104	103	151	129	122	120	
V_{REX}(s)	98(2)	68(2)	38(1.8)		81(2.2)	28(2.5)	2(1.4)		40(1.4)				47(2)		19(1.7)	20(2.7)
	100(4)	98(8)			99(8)		25(14)		95(8.1)				100(8)		31(31)	51(8.7)
		100(120)					65(31)		100(30)						100(120)	92(30)
							98(120)									100(118)
SFE	28.6		19.73			65.5		33.3		32.9		50		50		54

**Initial grain diameter (μm), D_0, and flow stress (MPa), σ (determined at a $\dot{\varepsilon}$ of 1 s^{-1} and a ε of 0.1 at 1150 °C), percent volume recrystallized with the associated hold time in seconds (Shown in parenthesis), V_{REX} (s), and SFE (mJ/m^2) for various wrought (and annealed) stainless steels. SFE was calculated according to Schramm and Reed[42] as follows: $\gamma = -53 + 6.2(Ni) + 0.7(Cr) + 3.2(Mn) + 9.3(Mo)$ for the first five alloys. SFE for A-286 is from Thompson and Brooks,[43] 903 from Novak,[44] and 22-13-5 estimated from the works of Schramm and Reed[42] and Stoltz.[45]

materials exhibited higher flow stress and so greater adiabatic heating during compression could enhance recrystallization. However, calculations showed that the maximum temperature difference between the two materials was minimal, on the order of 4 °C to 5 °C.

In addition to the wrought 316L, several other wrought austenitic stainless steels (elemental compositions given in Table VII) were also introduced into the study to provide further examination of the role of SFE and initial grain size in recrystallization. The alloys were annealed and similarly compressed and recrystallization results are presented in Figure 12(a) and Table VIII. The t_{50} was estimated for all of the alloys (from Figure 12(a)) and plotted *vs* D_o in Figure 12(b). It can be seen in the figure that the time for recrystallization decreases with decreasing D_o, for the 304L and 316L wrought materials, and that the various wrought alloys of roughly equivalent D_o separate according to SFE, which was calculated or reported,[42–45] the higher SFE being associated with longer times for recrystallization. Also shown in Figure 12(b) is the data point for as-cast 316L studied here. Although its SFE is approximately 50 mJ/m^2, t_{50} lies well above the band of SFE for the wrought alloys. To fall within the band at the appropriate SFE level, the effective grain size would seemingly have to be increased from the range of 55 to 95 μm, which was calculated from the microstructural features, to about 600 μm. However, the light microscopy and TEM observations demonstrate the important role of the delta ferrite in recrystallization, reinforcing the notion of a relatively fine effective grain size in the starting as-cast material.

A decrease in the effectiveness of the δ/γ boundaries in promoting recrystallization during thermal-mechanical treatment could be anticipated due to the dissolution (Figure 11(a)) and spheroidization (Figures 5 and 10) of the δ with time after deformation. It seems that movement of the δ boundaries away from the incipient sites of nucleation created by deformation may render these sites impotent. Another factor, which could account for the sluggish behavior of the as-cast material during later stages of recrystallization, is the apparent pinning effect that the δ has on the recrystallized grain boundaries (Figure 5). Finally, the effect of partitioning of alloying elements to δ and γ on a local scale could be considered. For example, the dissolution of δ will result in an adjacent γ matrix enriched in

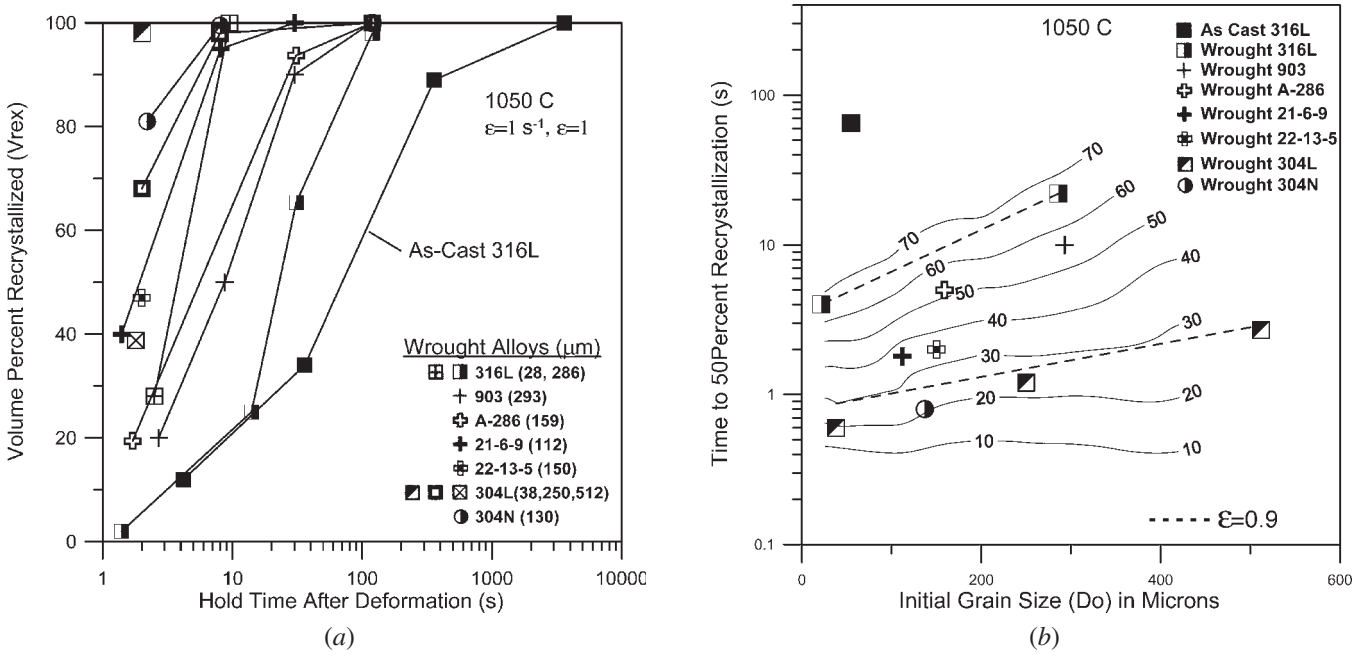

Fig. 12—The behavior of various austenitic stainless steels shows the role of stacking fault energy (SFE) in recrystallization: (*a*) the variation in V_{REX} with time. From the data in (a), the time for V_{REX} = 50 pct, t_{50}, was determined and plotted in (b); (*b*) the variation in t_{50} with initial grain size. The contours of SFE (mJ/m^2), plotted from the data in Table VIII, show that the as-cast 316L recrystallization kinetics are slower than expected for the effective grain size range (55 to 95 μm) calculated from the volume fraction and morphology of the δ. Only one data point for effective grain size is plotted, 55 μm.

Mo and Cr. This, in turn, could raise the local SFE as well as lower grain boundary mobility, favoring austenite recovery over recrystallization and grain growth in this local area during the later stages of recrystallization. Despite these various proposals of the role that the evolution of δ could play in the recrystallization kinetics, the results in Figure 11(b) indicate that the dissolution of δ does not have an overriding effect since most of it occurs after substantial recrystallization.

In the next section, the sluggish recrystallization kinetics of the as-cast 316L are deemed to be related, at least in part, to the "soft" orientation of the crystallographic texture with respect to the compression axis and a concomitant reduction in the rate of accumulation of dislocation density in the evolving substructure.

B. *Mechanical Behavior: The Role of Crystallographic Texture*

Texture can also play a dominant role in deformation behavior at high temperature. For example, the measured flow stress of fcc columnar grain structures has been shown to be sensitive to their orientation with respect to the axes of principle stress.[4,46] The common growth direction for primary dendrites is <100>. In fcc materials, the favored slip system is {111}<110>, although as temperature increases, other slip systems begin to operate, *i.e.*, {100}<110> and {110}<110>. If the compression axis is aligned with the columnar grain axes, as it was in this investigation, or perpendicular to the columnar grains, the {111} slip planes are favorably oriented with respect to the critical resolved shear stress, giving a "soft" orientation. Thus, flow stress for these orientations will be lower than orientations where the columnar axes lay at intermediate angles to the compression axis, *e.g.*, 45 deg, or to a condition with no preferred crystallographic texture, *e.g.*, a randomly oriented equiaxed grain structure.

The Taylor factor, M, is a measure of the average misorientation between the active slip planes and directions in an embedded crystal and the applied stress. In effect, M is inversely related to the effectiveness of the resolution of the applied stress onto the active slip planes in the slip directions of an embedded crystal. That is, for an applied stress, a crystal orientation giving a higher average resolved stress onto the slip planes in the slip directions will have a lower M value. For axisymetric flow, as in the axial tension or compression of rods, Chin[47] defines M for an embedded crystal as

$$M = \frac{\Sigma\gamma_1}{\varepsilon_x} = \frac{\sigma_x}{\tau^*} \qquad [7]$$

where γ_1 is glide shear, ε_x is axial strain, σ_x is the applied axial stress, and τ^* is the critical resolved shear stress. Knowing M for two cases, Eq. [7] can be used to obtain a ratio of the flow stress for two crystals of differing orientation. The two cases of interest here would be grains with the 100 orientation parallel to the axial stress, representing compression of the as-cast 316L, and grains with random orientation, representing deformation of the wrought 316L. For fcc crystals with {111}<110> slip, Chin[47] calculates the corresponding M values to be 2.449 and 3.067, respectively. The resultant ratio of the two flow stesses ($\sigma_{100}/\sigma_{random}$), as-cast to wrought, is 0.7985.

To make such a comparison, the flow stress of both as-cast and wrought 316L was measured at 1150 °C after a ε of 0.1. The flow stress of the cast material was approximately

76 MPa, while the flow stress of the fine and coarse grain wrought materials were 110 and 95 MPa, respectively. The corresponding $\sigma_{100}/\sigma_{\text{random}}$ ratios are 0.69 and 0.80, which agree fairly well with the predicted value of 0.7985. Thus, the relatively low flow stress of the as-cast 316L is consistent with the parallel orientation of the 100 columnar grain axes with the compression axis.

Flow stress is generally recognized to vary with dislocation density, which in turn evolves towards a steady state through competition between athermal work hardening, which occurs *via* dislocation generation and storage, and temperature- and strain-rate-dependent work softening, which occurs by dislocation annihilation.[48,49,50] Because recrystallization kinetics also vary with the accumulated dislocation density, the relatively sluggish recrystallization behavior of the as-cast 316L could be related, at least in part, to a reduced accumulation of dislocation density with applied strain as a result of a reduced Taylor factor. Miller and Dawson[51] recognized that, in general, to accommodate the same effective plastic strain rate, a smaller average Taylor factor implies less crystallographic slip activity. Thus, for the same applied strain rate, the dislocation density in the as-cast 316L would be expected to increase at a reduced rate compared to that in the randomly oriented 316L. Although the dislocation density was not measured in this study, the stress-strain behavior of the two materials at 1150 °C (not shown) reflects the expected behavior, *i.e.*, the hardening rate of the as-cast 316L was less than the randomly oriented 316L, at least up to a strain of approximately 0.5. Above 0.5, the flow stress of the random material saturated, indicating saturation of the dislocation density, while the as-cast material continued to harden, indicating continued evolution of the dislocation density (and substructure), assuming geometric hardening[51] is negligible. Despite continued hardening, the flow stress, and presumably the dislocation density, of the as-cast material never achieved that of the random material.

In order to predict recrystallization kinetics, Goerdeler and Gottstein[52] relate the evolution of the dislocation accumulation in the substructure to mobile dislocation density and express the applied strain rate as a function of the rate of generation of mobile dislocation density, based on the Orowan relationship, as follows:

$$\frac{\Delta\varepsilon}{\Delta t} \cong \dot{\varepsilon} = \dot{\rho}_m \mathbf{b} L_{eff}\left(\frac{1}{M}\right) \qquad [8]$$

where ε is applied strain, L_{eff} is the effective mean free path, **b** is Burgers vector, $\dot{\rho}_{\text{m}}$ is mobile dislocation density, and M is the polycrystal Taylor factor, where a dot signifies rate and a bar means average. Thus, during an increment of time, a dislocation density of $\dot{\rho}_{\text{m}}$ (Δt) is produced and those dislocations travel a distance of L_{eff}, at which point the dislocations form dipoles or locks, or are annihilated. Assuming the rate of annihilation is less that that of production, the evolving dislocation density in the substructure is proportional to the Taylor factor. For a constant applied strain rate, as M is reduced, the rate of generation of mobile dislocations is also reduced. Similar to the ratio of flow stresses for 100 randomly oriented crystals developed previously, the ratio of the rate of generation of mobile dislocations, and, thus, the ratio of the rate of accumulation of dislocation density in the substructure, between the two conditions is equal to the ratio of the Taylor factors, assuming L_{eff} is constant during the time increment considered and equivalent for the two materials, as follows:

$$\frac{M_{100}}{M_{\text{random}}} = \frac{\dot{\rho}_{m(100)}}{\dot{\rho}_{m(\text{random})}} = 0.7985 \qquad [9]$$

Thus, it is proposed that the sluggish recrystallization kinetics of the as-cast 316L, observed in Figure 12(b), is due, at least in part, to a reduced rate of accumulation of dislocation density in the substructure, which, in turn, is due to the 100 orientations of the columnar grain structure with respect to the compression axis.

With respect to the microstructure of the slab-type ingot studied here, large regions of the as-cast ingot are composed of columnar grains, which are aligned with the 100 orientations parallel to the compression axis in rolling. Thus, the recrystallization kinetics during primary breakdown of the 316L ingot can be expected to be sluggish during the initial stages of breakdown compared to the kinetics during subsequent processing, after the first wave of recrystallization has randomized the crystallographic texture.

C. *Application to Production Processing*

The data for as-cast 316L from Table V is presented in Figure 13 in a format that could facilitate process design by identifying conditions that obtain the desired initial wave of recrystallization during primary breakdown. The figure shows the variation in degree of recrystallization, plotted as iso-volume-fraction-recrystallized contours, for combinations of strain and temperature. Two sets of contours are shown, one for a hold time of 36 seconds (dashed lines), representing the earliest stages of ingot breakdown, for example, after one or two passes, and one for 3600 seconds (solid lines), representing an in-process reheat. During the earliest stages of thermal-mechanical treatment, recrystallization is enhanced by both greater strain and higher temperature. However, relatively large strains on the order of 0.5 at 1150 °C are needed to achieve a significant degree (25 pct) of recrystallization in 36 seconds of hold time. Typically, the strains imparted during ingot rolling range from 0.05 to 0.10 per pass, so significant recrystallization would not be expected during the first or second rolling pass. That stage in the process at which 25 pct recrystallization would be achieved, assuming deformation at 1150 °C, can be estimated from Figure 13 by interpolating between the 36 and 3600 second 25 pct contours. It appears that a ε of about 0.35 is needed at an intermediate time, *e.g.*, 120 seconds, which would correspond to about five passes of 0.07 strain per pass and a cycle time in a reversing rolling mill of 24 seconds (which is typical). If an in-process 3600 second reheat were employed early in the schedule to improve hot workability, a total applied ε of only about 0.15, which corresponds to about two or three passes, could be applied at 1150 °C to achieve 25 pct recrystallization. This type of analysis, albeit approximate, could also be applied to ingot breakdown by pressing or radial forging. Compared to rolling, both techniques involve greater redundant deformation per pass, better maintenance of temperature, larger reductions

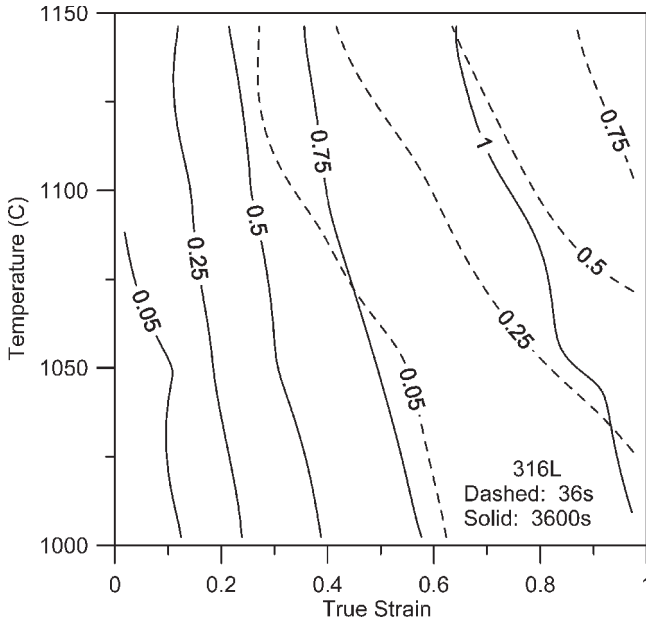

Fig. 13—Recrystallization map showing V_{REX} contours for two hold times, 36 s (dashed curves) and 3600 s (solid), plotted for combinations of temperature and strain.

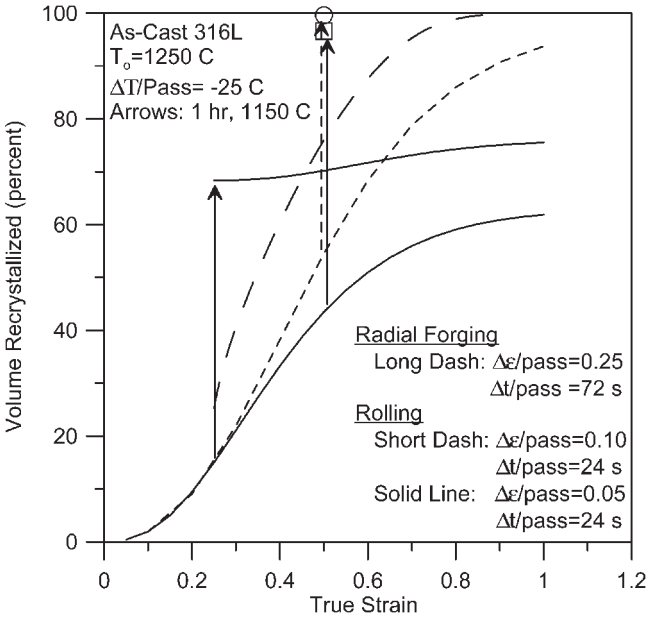

Fig. 14—Simulation of the evolution of V_{REX} with strain, *via* Eq. [6], and the experimentally determined constants in Table VI, for three primary breakdown techniques: radial forging, rolling with moderate strain/pass, and rolling with small strain/pass. Vertical arrows show the added recrystallization gained by an in-process heat treatment at 1150 °C for 1 h.

in cross section per pass, and longer interpass hold times, all factors which stimulate recrystallization.

Figure 14 presents more detailed modeling of the evolution of recrystallization during complex, multiple pass processes. For this purpose, Eq. [6] was employed with the fitted parameters from Table VI. A separate description of the recovery kinetics in as-cast 316L was beyond the scope of this investigation, so the volume fraction recrystallized (X_v) during successive interpass periods of time is calculated on the basis that strain in the unrecrystallized volume of microstructure is cumulative, *i.e.*, recovery does not occur during the interpass hold times. Cooling during successive passes is considered in the modeling. Regarding cooling, it is assumed that the total accumulated strain, from the prior passes, in the unrecrystallized portion of the microstructure is applied at the current deformation temperature; *i.e.*, strain applied at higher temperature in a previous pass is as effective in promoting recrystallization as the strain applied at a lower temperature during a later pass. Although the two assumptions lead to an overestimation of X_v, the relative behaviors of various processes can be compared. For example, Figure 14 shows the evolution of recrystallization, predicted *via* Eq. [6], during primary breakdown for three industrial techniques, *i.e.*, rolling with relatively low strain per pass, rolling with medium strain per pass, and radial forging with large strain per pass. For an initial deformation temperature of 1250 °C and a temperature drop of 25 °C per pass, the accumulated recrystallization after a total ε of 1 increases as the strain/pass is increased giving V_{REX} values of 62, 94, and 100 pct, respectively, for the three processes.

The effects of an intermediate reheat can be considered. For example, a 1 hour, 1150 °C reheat after five passes of the 20 pass schedule, giving a total ε of 0.25, results in about 68 pct recrystallization (shown by the vertical arrow in Figure 14). Note, however, that little recrystallization (an additional 7 pct) occurs during the subsequent fifteen passes, which resume at 1150 °C, because the accumulated strain in the unrecrystallized portion of the microstructure is assumed to be totally recovered during heat treatment. Application of a 1 hour, 1150 °C reheat after ten passes, instead of five, results in greater V_{REX}, 89 pct *vs* 68 pct, due to the greater applied strain, 0.5 *vs* 0.25. The intermediate heat treatment after five passes may improve workability early in the rolling schedule, but the total recrystallization achieved is less than if the reheat is applied after ten passes. The precise role of delta ferrite as it evolves in morphology and dissolves is not considered nor predicted in the preceding analysis, but its effect on recrystallization kinetics is incorporated in the constants in Eq. [6], which was fitted to the measured data.

The downward curvature in the curves in Figure 14 is due mainly to interpass cooling, which suppresses recrystallization during later passes. Assuming a greater cooling/pass would accentuate the downward curvature. Such dependency might be observed during rolling of as-cast products with differing cross-sectional geometry. For example, thicker bottom poured ingots (*e.g.*, 60-cm thick) would cool less quickly than continuously cast slabs (approximately 15-cm thick) and would exhibit less downward curvature.

Not considered in the preceding predictions is the redundant work that is applied to the workpiece by radial forging, which would in effect increase the magnitude of the accumulated strain in the microstructure beyond that assumed here, calculated simply by the measured reduction in cross-sectional area. Considering this, the predicted recrystallization during radial forging may be underestimated in Figure 14. A better estimate of the progression of recrystallization during radial forging could be obtained by coupling the kinetic model with finite-element analysis of the forging process.

V. CONCLUSIONS

1. The as-cast 316L microstructure is consistent with solidification by primary ferrite followed by secondary solidification of austenite (F/A type solidification). After solidification, there is also some transformation of ferrite to austenite. Delta ferrite remains at the original cores of the primary and secondary dendrite arms and its morphology is generally vermicular (skeletal). The measured volume fraction of ferrite in the as-received ingot, 4.4 pct, and the F/A type of solidification agrees well with predictions using Cr and Ni equivalents developed for solidification of stainless steel weld pools.
2. Alignment of the compression axis with the axes of the columnar grains gives uniform flow during compression. Because this orientation favors slip, the measured flow curves are low compared to those measured for wrought 316L with an equiaxed grain structure with random texture. The observed sluggish recrystallization of as-cast material compared to wrought material could not be explained by differences in starting grain size or SFE, but is consistent with a reduced rate of accumulation of dislocation density in the evolving substructure that occurs because the axes of the columnar grains, which have a 100 crystallographic orientation, are aligned with the compression axis. The compressive strain applied in rolling is similarly oriented with respect to the columnar grains in bottom-poured slab type ingots and, thus, rolling stresses will be lower than predicted from deformation studies conducted on randomly oriented structures and that would be encountered once the initial wave of recrystallization is complete.
3. The monotonic increase observed in the flow curves demonstrates that dynamic recrystallization is not a dominant grain refinement mechanism during primary breakdown. Static recrystallization is the dominant mechanism with the greatest majority of the nucleation events taking place at the δ/γ boundaries and some occurring at the columnar grain boundaries.
4. The rate of static recrystallization in as-cast 316L can be modeled with Avrami-based kinetics. The best fit of the data was obtained with an Avrami exponent of about 0.5, which is at the low end of the spectrum typically observed, 0.5 to 2.0. The relatively low value is attributed to the inhomogeneous nature of recrystallization and to the evolution of the δ microconstituent. The δ/γ interface supplies a large boundary area for the nucleation of recrystallization, at least during the early stages of processing. With deformation and time, however, δ proceeds to spheroidize and dissolve. Movement of the δ/γ boundaries may leave incipient nuclei impotent. In addition, dissolution should enrich the adjacent matrix in Cr and Mo, thereby raising the SFE in the matrix immediately adjacent to the δ/γ boundary. If so, one would expect an increased propensity for recovery in the very area that provides the recrystallization nuclei.
5. The observed difference in recrystallization rate between as-cast and wrought 316L was much less than observed for 304L in two separate studies, in the literature. This is attributed to the presence of a relatively large volume fraction of delta ferrite and its vermicular morphology, which, together, provide a fine effective grain size and ample sites for recrystallization in the as-cast 316L studied here. In the two literature studies, the 304L was homogenized prior to the study, a processing step that spheroidized and greatly reduced the volume of delta ferrite, yielding a much larger effective grain size than observed here. A homogenizing treatment was not employed here, because it is not the common industrial practice.
6. The data generated in the study are useful in determining the effects of various processing schedules on the extent of recrystallization, especially through the use of the mathematical model developed here, Eq. [6]. The analysis presented here could be improved should the recovery kinetics of as-cast 316L be determined or the kinetic relationship(s) be coupled with the evolving gradients in strain, strain rate, and temperature availed by finite-element analysis.

ACKNOWLEDGMENTS

The authors thank Dr. Fred Fletcher, Bethlehem Steel Corp. (formerly with Lukens Steel Co.) for providing the material and information regarding primary breakdown procedures; Dr. David Matlock, Director of the Advanced Steel Processing and Product Research Center (ASPPRC), Colorado School of Mines (CSM), for guidance; Roger Jaramillo (CSM) for help in modeling the recrystallization behavior; Dr. David Olsen (CSM) for helpful discussions regarding solidification phenomena in stainless steels; Dr. Matthew Miller, Cornell University, for discussions on texture effects; Bob McGrew (CSM) for help with SEM and TEM; Terri Abeln and Ann Kelly, Los Alamos National Laboratory (LANL), for help in developing appropriate polishing and etching procedures for light microscopy; and Victor Vargas (LANL) for help with compression testing. We also acknowledge the sponsors for their contributions to the ASPPRC, an industry/university cooperative research center, as well as the Department of Energy's Los Alamos National Laboratory and Rocky Flats Plant for support.

REFERENCES

1. H.J. McQueen and J.J. Jonas: *J. Appl. Metalworking*, 1984, vol. 3 (3), pp. 233-41.
2. W. Roberts: in *Deformation, Processing and Structure*, G. Krauss, ed., ASM, Metals Park, OH, 1984, pp. 109-84.
3. W. Roberts, H. Boden, and B. Ahlblom: *Met. Sci.*, 1979, Mar.–Apr., pp. 195-205.
4. M.C. Mataya, M.L. Robinson, D. Chang, M.J. Weis, G.R. Edwards, and D.K. Matlock: *29th Mechanical Working and Steel Processing Conf. Proc.*, ISS-AIME, Toronto, ON, Canada, 1987, vol. XXV, pp 235-248.
5. S.L. Semiatin, G.D. Lahoti, and T. Altan: *Process Modeling-Fundamentals and Applications to Metals*, ASM, Metals Park, OH, 1980, pp 387-408.
6. G.T. Campbell, JR., E.P. Abrahamson, and N.J. Grant: *Metall. Trans.*, 1974, vol. 5, pp. 1875-81.
7. R.H. Kane: in *The Hot Deformation of Austenite*, J.B. Balance, ed., AIME, New York, NY, 1977, pp. 457-498.
8. N.D. Ryan and H.J. McQueen: *New Developments in Stainless Steel Technology*, ASM, Metals Park, OH, 1985, pp. 293-304.
9. E.R. Nilsson: Master's Thesis, Colorado School of Mines, Golden, CO, 2000.
10. M.C. Mataya and V.E. Sackschewsky: *Metall. Trans. A*, 1994, vol. 25A, pp. 2737-52.
11. D.J. Long and W.T. Delong: *Welding J.*, 1973, vol. 52, (7), pp. 281s-297s.

12. D. Kotecki and T.A. Siewert: *Welding J*., 1992, vol. 71 (5), pp. 171s-179s.
13. E.L. Brown: in *Materials Studies for Magnetic Fusion Energy Applications at Low Temperatures—IV*, National Bureau of Standards, Boulder, CO, 1981, pp. 357-414.
14. E.F. Boultbee and G.A. Schofield: *Typical Microstructures of Cast Metals*, Institute of British Foundrymen Publications, Birmingham, England, 1981, pp. 210-15.
15. K. Kuo: *J. Iron Steel Inst*., 1954, Apr., pp. 433-41.
16. N. Suutala: *Metall. Trans. A*, 1982, vol. 14A, pp. 191-97.
17. O. Hammer and U. Svennson: *Solidification and Casting of Metals*, The Metals Society, London, 1979, pp. 401-10.
18. N.D. Ryan, H.J. McQueen, and J.J. Jonas: *Can. Metall. Q*., 1983, vol. 22 (3), pp. 369-78.
19. S.A. Saltykov: in *Stereology*, H. Elias, ed., Springer-Verlag, New York, NY, 1967.
20. B. Weiss and R. Stickler: *Metall. Trans*., 1972, vol. 3, pp. 851-66.
21. K.W. Andrews, D.J. Dyson, and S.R. Keown: *Interpretation of Electron Diffraction Patterns*, Plunum Press, New York, NY, 1971.
22. J.W. Edington: *Practical Electron Microscopy in Materials Science*, Van Nostrand Reinhold, 1976.
23. G. Kurdjumov and G. Sachs: *Z Phys*., 1930, vol. 64, pp. 325-43.
24. Z. Nishiyama: *Sci. Rep. Res. Inst., Tohoku Univ*., 1934, vol. 23, pp. 637-64.
25. G. Wasserman: *Arch. Eisenhuttenwes*., 1933, vol. 16, p. 647.
26. T.J. Headley and J.A. Brooks: *Metall. Mater. Trans. A*, 2002, vol. 33A, pp. 5-15.
27. E.L. Brown, T. Whipple, and G. Krauss: *Duplex Stainless Steels*, ASM, Metals Park, OH, 1980.
28. A. Pinol-Juez, A. Iza-Mendia, and I. Gutierrez: *Metall. Mater. Trans. A*, 2000, vol. 31A, pp. 1671-77.
29. D.R. Barraclough and C.M. Sellars: *Metal Sci*., 1979, Mar.–Apr., pp. 257-67.
30. J.P. Sah, G.J. Richardson, and C.M. Sellars: *Metal Sci*., 1974, vol. 8, pp. 325-31.
31. M.C. Mataya, E.R. Nilsson, and G. Krauss: in *Superalloys 718, 625, 706, and Various Derivatives*, E.A. Loria, ed., TMS, Warrendale, PA, 1994, pp. 331-43.
32. M.C. Mataya: *J. Met*., 1999, vol. 51 (1), pp. 18-26.
33. M.C. Mataya and D.K. Matlock: in *Superalloy 718, Metallurgy and Applications*, E.A. Loria, ed., TMS, Warrendale, PA, 1989, pp. 155-78.
34. A.R. Jones: *J. Mater. Sci*., 1981, vol. 16, pp. 1374-80.
35. J. Huber and M. Hatherly: *Met. Sci*., 1979, vol. 13, pp. 665-69.
36. H. Hu, B.B. Rath, and R.A. Vandermeer: in *Recrystallization '90*, T Chandra, ed., TMS, Warrendale, PA, 1990, pp. 3-16.
37. C.M. Sellars and J.A. Whiteman: *Met. Sci*., 1979, vol. 13, pp. 187-94.
38. D.J. Towle and T. Gladman: *Met. Sci*., 1979, vol. 13, pp. 246-56.
39. I. Kozasu and T. Shimizu: *Trans. Iron & Steel Inst., Jpn*. 1971, vol. 11, pp. 359-66.
40. F.J. Humphreys and M. Hatherly: *Recrystallization and Related Annealing Phenomena*, Elsevier Science Ltd., New York, NY, 1996.
41. F. Ahlblom: "A Metallographic Study of Recrystallization After Hot Working in an 18/8 Austenitic Stainless Steel," Report No. IM-1210, Swedish Institute for Metal Research, Apr. 1977, pp. 1-27.
42. R.E. Schramm and R.P. Reed: *Metall. Trans. A*, 1975, vol. 6A, pp. 1345-50.
43. A.W. Thompson and J.A. Brooks: *Metall. Trans. A*, 1975, vol. 6A, pp. 1431-42.
44. C.J. Novak: in *Handbook of Stainless Steels*, D. Peckner and I.M. Bernstein, eds., McGraw-Hill Book Company, New York, NY, 1977, pp. 4-1-4-78.
45. R.E. Stoltz and J.B. Vander Sande: *Metall. Trans. A*, 1980, vol. 11A, pp. 1033-37.
46. M.J. Stewart: *Metall. Trans. A*, 1975, vol. 6A, pp. 1672-74.
47. G.Y. Chin: *The Inhomogeneity of Plastic Deformation*, ASM, Metals Park, OH, 1973, pp. 83-112.
48. U.F. Kocks: *J. Eng. Mater. Technol*., 1976, vol. 98, pp. 76-85.
49. H. Mecking and U.F. Kocks: *Acta Metall*., 1981, vol. 29, pp. 1865-75.
50. Y. Estrin and H. Mecking: *Acta Metall*., 1984, vol. 32, pp. 57-70.
51. M. Miller and P. Dawson: *J. Mech. Phys. Solids*, 1997, vol. 45 (11-12), pp. 1781-804.
52. M. Goerdeler and G. Gottstein: in *Recrystallization and Grain Growth*, G. Gottstein and D.A. Molodov, eds., Springer-Verlag, NewYork, NY, 2001, pp. 987-94.